

**SYNTHESIS OF HIGH-PERFORMANCE SUPERCAPACITOR  
ELECTRODES USING A CNT-ZIF-MOS<sub>2</sub> FRAMEWORK**

by

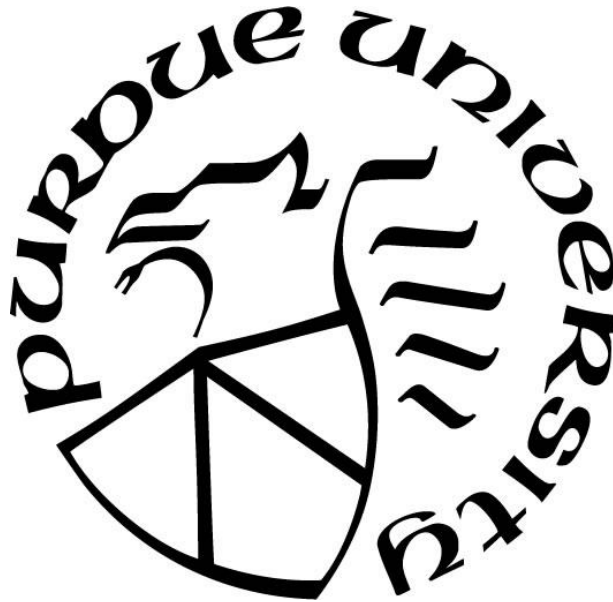
**Duncan Neal Houpt**

**A Thesis**

*Submitted to the Faculty of Purdue University*

*In Partial Fulfillment of the Requirements for the degree of*

**Master of Science in Mechanical Engineering**



School of Mechanical Engineering

West Lafayette, Indiana

May 2020

**THE PURDUE UNIVERSITY GRADUATE SCHOOL  
STATEMENT OF COMMITTEE APPROVAL**

**Dr. Jong Hyun Choi**

School of Mechanical Engineering

**Dr. Kejie Zhao**

School of Mechanical Engineering

**Dr. Liang Pan**

School of Mechanical Engineering

**Approved by:**

Dr. Nicole L. Key

*Dedicated to my wonderful family who have always been supportive of me throughout my long academic journey. Thank you to my mom Barb, my dad James and my siblings Briana and Brogan.*

*Also dedicated to my incredible friends who have been by my sides through the ups and downs of life. Thank you for always having my back and helping me pull through numerous all-nighters and stressful times in school.*

## **ACKNOWLEDGMENTS**

Thank you, Professor Choi, for your constant guidance throughout both my undergraduate and graduate time here at Purdue University. Your mentorship has been very well appreciated and I thank you for all the time and effort that you have invested into me and the research we have done together. Additionally, I would like to thank and acknowledge the United States National Science Foundation for funding the research presented in this thesis presentation. I would also like to thank Professors Zhao and Pan for agreeing to serve as members of my committee and for giving me good feedback on my project and the direction of my research.

I would also like to thank Jaehoon Ji who has also helped to mentor throughout my time at Purdue and who has helped me with numerous of the experiments that I have conducted in my time here at Purdue. And I would also like to thank Daniel Yang for assisting in some of the experiments as an undergraduate student.

# TABLE OF CONTENTS

LIST OF TABLES .....	7
LIST OF FIGURES .....	8
ABSTRACT .....	11
1. INTRODUCTION .....	12
1.1 Energy Usage Growth.....	12
1.2 Renewable Energy Generation .....	12
1.3 Energy Storage.....	13
1.4 Electrochemical Energy Storage.....	14
1.5 Supercapacitors .....	15
1.6 Scope of the Thesis .....	16
2. LITERATURE REVIEW .....	17
2.1 Materials .....	17
2.1.1 Carbon Based Materials.....	17
2.1.2 Metal Organic Frameworks .....	22
2.1.3 Transition Metal Dichalcogenides.....	23
2.2 Energy Storage Devices .....	25
2.2.1 Electrochemical Energy Storage Technologies .....	25
Battery .....	28
History.....	28
Theory .....	28
Modern Research .....	30
Supercapacitor .....	31
History.....	31
Theory .....	32
Hybrid/Asymmetrical Devices .....	39
3. MATERIALS AND METHODS .....	41
3.1 Synthesis of CNT, ZIF-8, MoS <sub>2</sub> Framework .....	42
3.2 Electrochemical Testing.....	46
3.3 Choice of Current Collector.....	51

3.4	Choice of Electrolyte .....	54
4.	RESULTS AND DISCUSSION.....	56
4.1	SEM Imaging .....	56
4.2	Theoretical Capacitance Calculations.....	61
4.3	Electrochemical Measurements .....	62
4.3.1	Highest Performing Sample Measurements .....	62
4.3.2	Variable Scan Rates Results .....	66
4.3.3	Analysis of ratio of MoS <sub>2</sub> : ZIF-8 ratio.....	68
4.3.4	Analysis of ratio of ZIF-8 : Carbon Nanotubes .....	70
4.3.5	Comparison of Materials at Every Phase of Production.....	73
5.	CONCLUSION AND FUTURE WORK .....	76
5.1	Conclusions.....	76
5.2	Future Work Considerations .....	77

## LIST OF TABLES

Table 2.1 Comparison of the properties of SWCNTs and MWCNTs. Reused from [6] N. Saifuddin et. al.....	21
Table 2.2. Comparison of supercapacitor research being done on many different nanomaterials. .....	38
Table 4.1. Table comparing values of the mass ratio of MoS <sub>2</sub> to ZIF-8 to capacitance.....	69
Table 4.2 Table comparing values of the mass ratio of carbon nanotubes to ZIF-8 to capacitance. .....	71
Table 4.3. Comparison of the performance of the sample at several different stages of production .....	73

## LIST OF FIGURES

- Figure 2.1. This figure shows the different allotropes of nanoscale carbon as well as their number of dimensions that are larger than the nanoscale. Image from [5], all rights and permissions inquiries should be directed towards ACS..... 18
- Figure 2.2. This illustrates the different methods by which graphene can be rolled to create carbon nanotubes with the three structural types of carbon nanotube (armchair, zigzag, and chiral) on display as well as A, B, and C, respectively. Image from [9] rights and permissions granted from Elsevier who should be contacted for all future rights or permissions inquiries..... 20
- Figure 2.3. Image of the structure of a metal organic framework. Note the bonding between the organic ligands and metal nodes which make the characteristic structure. Used with permission from [15] with all rights and permissions held by Elsevier ..... 23
- Figure 2.4. Demonstration of the structure and bonding of MoS<sub>2</sub> and other transition metal dichalcogenides with both crystalline structures, 2H and 1T, shown. Figure taken from [27] with rights and permissions granted by Springer Nature who owns the copyright of the material. .... 25
- Figure 2.5. Schematic of a typical electrochemical energy storage system..... 26
- Figure 2.6. Ragone chart depicting the specific power and specific energy of various popular electrochemical energy storage devices. Notice that the values of the supercapacitors typically stretch from a specific power of between 100 and 30000 W/kg and energy density ranging from 0.1 to 8 Whr/kg. This figure is taken from [28] image used with the rights and permissions from ACS publishing..... 27
- Figure 2.7. Schematic of a typical electrochemical battery cell. Note that the direction of the ion flux varies depending on whether the device is charging or discharging. Figure reproduced from [29] written by Zhang et al who own the copyright on the material and hosted by IEEE..... 29
- Figure 2.8. Ragone chart demonstrating the specific energy and power of common types of batteries as well as popular battery research technologies such as metal air batteries. Image taken from [31] with rights and permissions granted by Springer Nature who should be contacted regarding further uses of the copyright..... 31
- Figure 2.9. Image of the electrostatic double layer capacitor electrochemical cell showing all of the components necessary including the optional separator. This image is used from [33] with the right and permissions granted from Elsevier. .... 33
- Figure 2.10. Cyclic voltammetry and galvanostatic charge-discharge graphs for three different energy storage devices: battery, supercapacitor, and a hybrid battery-supercapacitor system. Of special note is the shape of the different graphs, battery electrodes have oxidation peaks and have plateaus during charge-discharge testing, supercapacitors exhibit box-like cyclic voltammetry and linear charge-discharge graphs. Figure is used from [4] from George Chen hosted by Taylor and Francis..... 36
- Figure 2.11. Comparison of charge-discharge performance of pseudocapacitor, supercapacitor, and battery electrodes. Figure taken from [4] from George Chen hosted by Taylor and Francis. 40

Figure 3.1 Overview of the material synthesis process. First a layer of polydopamine hydrochloride is applied to the carbon nanotubes. After that, ZIF-8 is bonded to the carbon nanotubes by bonding with the dopamine. Finally, few-layered MoS <sub>2</sub> flakes are deposited onto the ZIF-8 via disulfide bonding. ....	41
Figure 3.2. Process of synthesizing a carbon nanotube and ZIF-8 compound by using a polydopamine mediated process. Cited from [34] with rights and permissions granted by Elsevier publishing.....	43
Figure 3.3 Vacuum Filtration process used to remove solute from sample to deposit electrode material onto membrane. ....	44
Figure 3.4. Image of completed electrode deposited onto nickel foam using conductive epoxy. 45	
Figure 3.5. Image of electrochemistry testing bench.....	47
Figure 3.6. Image of 3 electrode electrochemical cyclic voltammetry test setup. The setup consisted of 1Ag/AgCl reference electrode, 1 platinum plate counter electrode, and the working electrode.....	48
Figure 3.7. Bleaching process by which the thin layer of AgCl is restored to the outer surface of the silver wire in the Ag/AgCl electrode .....	49
Figure 3.8. Picture of sample that had sat unused for a long time showing a large degree of sedimentation. ....	50
Figure 3.9. Image a sample shortly after being removed from the oven with a very well-dispersed consistency.....	51
Figure 3.10. Samples deposited onto copper tape that showed large degrees of corrosion.....	52
Figure 3.11. Pourbaix diagram of copper in aqueous solution (electrolyte) showing corrosive behavior at the pH of 6M KOH in water. Taken from [78] with permission from Springer Nature publishing.....	53
Figure 3.12. 6M KOH after various amounts of time performing cyclic voltammetry with copper tape substrate which exhibits a large degree of corrosion. ....	54
Figure 3.13. Figure showing the effect of electrolyte on the performance of the electrolyte on a Co(OH) <sub>2</sub> electrode. Used with permission of Elsevier under the <a href="http://creativecommons.org/licenses/by-nc-nd/4.0/">http://creativecommons.org/licenses/by-nc-nd/4.0/</a> from [80] .....	55
Figure 4.1. SEM images of the sample with only single walled carbon nanotubes at various magnifications of A (50x) and B (100x).....	58
Figure 4.2. SEM images of the sample ZIF-8 bonded to carbon nanotubes at various magnifications of A (50x) and B (100x).....	59
Figure 4.3. SEM images of the complete framework of CNT-ZIF-8-MoS <sub>2</sub> at various magnifications of A (50x) and B (100x).....	60
Figure 4.4. Cyclic Voltammetry graph showing the performance of the electrode at a scan rate of 20mv/s with a voltage window of 0 to -1.2V.....	62

Figure 4.5. Durability of the electrode over 30000 cycles. This shows relatively little degradation in performance over a larger number of cycles. Normalized against the value of the capacitance at 30000 cycles..... 65

Figure 4.6. Cyclic Voltammetry graph of the electrode at various scan rates to show the change in performance that can be achieved by altering the scan rate..... 66

Figure 4.7. Ragone chart with performance of the supercapacitor at various scan rates to show how energy and power change with scan rate from 100mV/s as the top point to 20mV/s as the point with the lowest power density..... 67

Figure 4.8. Ragone chart from the introduction with the point for the sample taken at 20mV/s graphed as well to show performance relative to other energy storage techniques. This figure is taken from [28] image used with the rights and permissions from ACS publishing..... 68

Figure 4.9. Figure of the plotted data from Table 4.1. showing the graphical relationship between performance and the ratio of MoS<sub>2</sub> to ZIF-8. .... 70

Figure 4.10. Figure of the plotted data from Table 4.2. showing the graphical relationship between performance and the ratio of CNT to ZIF-8..... 72

Figure 4.11. Cyclic voltammetry graph of 1 cycle for each material at various stages of production including CNT only, CNT-(ZIF-8), and CNT-(ZIF-8)- MoS<sub>2</sub>..... 74

Figure 4.12. Graph of only carbon nanotubes and molybdenum disulfide without the ZIF-8 present, notice that the capacitance of this data is also lower than the value of the combined material.... 75

## ABSTRACT

Supercapacitors are an emerging energy storage device that have gained attention because of the large specific power, at a reasonable specific energy, that they exhibit. These energy storage devices could be used alongside of or in the place of traditional electrochemical battery technologies to power reliable electrical devices. The performance of supercapacitors is largely determined by electrode properties including the surface area to volume ratio, the electrical conductivity, and the ion diffusivity. Nanomaterial synthesis has been proposed as a method of enhancing the performance of many macroscopic supercapacitor electrodes due to the high surface area to volume ratio and unique tunable properties that are often size or thickness dependent for many materials. Specifically, carbon materials (such as carbon nanotubes), metal organic frameworks, (such as ZIF-8), and transition metal dichalcogenides (such as molybdenum disulfide) have been of interest due to their conductivity, large surface area, and ion diffusivity that they exhibit when one or more of their characteristic lengths is on the order of several nanometers.

For the experiments, a carbon nanotube-/ZIF-8-/MoS<sub>2</sub> framework was synthesized into an electrode material. This process involved first dispersing the carbon nanotubes in DMF using ultrasonication and then modifying the structure with polydopamine to create a binding site for the ZIF-8 to attach to the carbon nanotubes. The ZIF-8 was synthesized by combining 1,2,4-Triazole-3-thiol and ZnCl under 120 degrees Celsius. Afterwards, the MoS<sub>2</sub> was associated with the carbon nanotube and ZIF-8 framework by a disulfide bond with the sulfur vacancy of the MoS<sub>2</sub> and the sulfide group of the ZIF-8. Finally, the sample solution was filtered by vacuum filtration and then annealed at 110 degrees Celsius before being deposited on a nickel foam substrate and tested in a 3-electrode electrochemical cyclic voltammetry study.

The resulting materials were found to have a capacitance of 262.15 F/g with corresponding specific energy and specific power values of 52.4 Whr/kg and 1572 W/kg. Compared to other supercapacitor research materials, this electrode shows a much larger capacitance than other exclusively carbon materials, and comparable capacitance values to the ZIF-8 and MoS<sub>2</sub> materials with the added benefits of an easier and faster manufacturing process. Overall, the electrodes developed in this study, could potentially reduce the cost per farad of the supercapacitor to be more competitive energy storage devices.

# **1. INTRODUCTION**

## **1.1 Energy Usage Growth**

As the world population grows and countries around the world continue to industrialize and become more dependent on technology, the world energy use increases. While 2020 was an outlier due to the economic halt created by the COVID-19 pandemic, world energy demand has grown steadily every year and projects to be 29000 TWh by 2030 [1]. This increase in energy demand will lead to an increase in the amount of energy produced as well. This increase in energy demand has traditionally not been a problem as the amount of energy produced has been easily scaled by discovering new ways to burn and discover fossil fuels and by making processes and devices more efficient. However, as the world continues to increase the amount of carbon producing energy fuels, we have seen a subsequent increase in global average temperature and other extreme weather conditions that scientists have predicted would arise because of global warming or the greenhouse effect from burning fossil fuels. According to the World Energy Outlook [1], the demand for carbon producing fuels was over 11000 Mtoe (megatons of oil equivalent) in 2019 which more than likely would significantly accelerate climate change and lead to drastic consequences. Scientists have warned that these rises in carbon emissions could lead to irreversible “tipping points” that may cause long lasting, irreversible consequences if left unchecked. The response to the looming climate catastrophe (because we cannot significantly decrease the amount of energy demanded) has to be to look at alternative sources of energy generation to meet our needs[2]. Several alternative “clean” energy generation methods, such as renewable energy technologies, nuclear, etc. have been proposed as a method for helping to take over the roles of carbon burning fuels as our primary energy source.

## **1.2 Renewable Energy Generation**

To combat the rise in carbon dioxide, countries around the world have entered into the Paris Climate Agreement, among taking other measures, to decrease carbon dioxide emissions. To reduce the amount of fossil fuels burned while also meeting the amount of energy demanded, renewable energy resources and other energy generation techniques (that do not emit carbon dioxide when utilized) must be used in increasing amounts. Technologies such as solar, wind,

geothermal, wave, nuclear, and many others will have to be utilized to their full potential in order to meet the increasing energy demands. It is predicted that the total amount of renewable resource energy demanded by 2030 will increase by nearly 50 percent and will likely continue at this accelerating pace into the future[1]. These resources have great potential to be able to meet the energy demands of the world, but there are several major limitations in their widespread use. Economically, the price of most renewable sources compared to fossil fuels is still high and this price must drop or even dip below the levels of fossil fuels to be adopted widely. There are several ways to decrease this price to make renewable energy resources more competitive with fossil fuels. One way to lower this price is to make the technology less expensive which is being explored in great length. An additional way is through improving the efficiencies of these technologies so that they generate more electricity from the natural resources that they are producing from which is also being explored. Another way, the method that most directly relates to this thesis, is by increasing the efficiency of the energy storage systems that will be necessary to store the energy produced from renewables for times when they are needed, as peak production hours for renewable energy sources do not often align with peak demand hours of the energy grid. Each of these methods will have to be explored for renewable energy technologies to produce the amounts of energy that are demanded of them. However, as previously mentioned, the method of improvement most relevant to this paper will be that of more efficiently storing energy for later use.

### **1.3 Energy Storage**

As mentioned above, switching the energy grid to utilize renewable energy resources also requires the increased use of energy storage technologies. One of the largest reasons why energy storage is required is intermittency, the result of renewable energy resources such as solar panels producing much of their energy at non-peak usage times throughout the day. This means the energy produced at optimal times, must be stored for use at different times of the day when the demand is highest and energy production is lowest (evening/night or winter). This brings with it several problems such as energy losses that accompany storage techniques and inefficiencies involved in transferring the electricity to and from a storage mechanism as well as problems of needing to provide both high power and high energy to meet sudden demand changes. This problem also requires long term energy storage techniques for when winter (or equivalent time periods of less solar radiation) occurs in a given area. To address these concerns, energy storage systems have

been purposed to store that energy temporarily until it is needed for use and are the subject of much current research. Generally, energy storage techniques can be generalized into 3 different categories, (mechanical, electrochemical, and thermal) based on the medium of energy storage. Mechanical energy storage stores energy in a mechanical process such as the spinning of a flywheel or pumped hydro (running a hydroelectric dam system in reverse) and requires minimizing the dissipating forces to minimize energy losses throughout the storage period. Thermal energy storage is often associated with space or water heating and involves heating some fluid either for residential use as in underground thermal storage for year-round space/water heating or for power generation such as in systems like concentrated solar supercritical vapor cycles. No matter their purpose, thermal energy storage systems are often dependent on the insulating materials used around piping and tanks to minimize the amount of heat loss from these components. Electrochemical energy storage systems are the most widely used type of energy storage as this encompasses many devices such as batteries and supercapacitors which store energy in chemical reaction and are used in many everyday electronic devices that are used such as mobile phones and personal computers. Oftentimes, these systems are composed of 2 electrodes, one positive and one negative, one or two different kinds of electrolyte, some kind of separator, and current collectors. Each of the methods in these broad categories has advantages and disadvantages, and generally can provide a combination of good energy or power or has other benefits and drawbacks. Due to the differing benefits and drawbacks of each of these systems, any future grid will more than likely have to include a combination of these different energy storage media and so all are likely to be important moving forward and the subject of much focus and research.

#### **1.4 Electrochemical Energy Storage**

As mentioned above, the most widely utilized form of energy storage today is that of electrochemical energy storage. Within electrochemical energy storage, batteries are by far the most widely utilized technology, being the primary energy storage for personal electronic devices such as cell phones and personal computers. Batteries are also under a great deal of research consideration now as the next generation of batteries with even greater energy and power densities are proposed and commercialized resulting in marked improvements in technologies such as electric cars. However, batteries as an energy storage medium have a relatively low power density

compared to their high energy density resulting in slower charging and discharging devices which are needed in all kinds of technologies, most notably transportation technologies. To bridge this gap, other forms of electrochemical energy storage are often used in parallel with batteries such as a capacitor or supercapacitor. Capacitors, opposite of batteries, have a very large power density but have incredibly small energy density which limits the applicability to a wide variety of fields. Supercapacitors are a form of energy storage that bridge the gap between capacitors and batteries by having relatively high power densities ( $\sim 1000$  W/kg) of traditional capacitors with much higher energy density ( $\sim 5$  Wh/kg) [3]. There have additionally been hybrid battery-supercapacitor devices which both a battery electrode and a supercapacitor electrode which potentially could lead to further improvements to performance [4]. Moving forward, a combination of these technologies will be required for both the electrification of the grid and the advancement of technologies such as the electric car or other electric transport devices.

## 1.5 Supercapacitors

Supercapacitors have historically been made of carbon-based materials such as activated carbon. The performance of supercapacitors requires a good electrical conductivity as well as a large energy storage potential and large surface area. These carbon-based materials all generally have a combination of these three abilities as well as being widely available materials which have made them the prevailing choice as materials for supercapacitors. These materials also have unique structures, that have pores or other features which have very high surface area to volume ratios.

Other materials have also been widely researched as supercapacitor electrode films which possess large surface areas and good conductivities similar to the carbon materials discussed above. One of the materials that has traditionally been studied both as a battery and a supercapacitor electrode is transition metal oxides (such as manganese dioxide  $\text{MnO}_2$ ). These films have been shown to have improved capacitance, as well as energy density and power density, when made into supercapacitor films. Molybdenum disulfide ( $\text{MoS}_2$ ) is a transition metal disulfide which has similar properties to the transition metal oxides discussed above and has even been shown to have properties that may make a good supercapacitor electrode such as a large surface area and a good energy capacity.

To improve upon these materials, it is hypothesized that combining carbon-based materials with other nanomaterials could further increase the surface area of the capacitor leading to higher

capacitances. Recently, many transition metal oxides (such as manganese dioxide  $\text{MnO}_2$ ) have been used for both battery and supercapacitor electrodes. These materials have even been combined with the carbon-based materials discussed above to make hybrid films showing improved electrochemical properties. Molybdenum disulfide ( $\text{MoS}_2$ ) is a transition metal disulfide which has similar properties to the transition metal oxides discussed above and has even been shown to have properties that may make a good supercapacitor electrode such as a large surface area and a good energy capacity. However, the material which has these properties is a highly unstable structure when it is only a few layers thin and bonds primarily through sulfur bonding. To effectively bind the carbon-based material and the transition metal dichalcogenide material, and intermediate of ZIF has been proposed as a framework to connect the carbon-based material and the TMDC material that has a large surface area but relatively low capacity and capacitance as well as a high ion diffusivity which can positively affect performance.

## **1.6 Scope of the Thesis**

To make a high energy and power density supercapacitor film, this project proposes to combine carbon nanotubes, ZIF-8, and molybdenum disulfide into a high performing supercapacitor film. It also proposes a much simpler manufacturing process that requires far lower temperatures and is quicker than other methods that have been proposed. The aim is to have an energy density on the order of magnitude of 100 Whr/kg (much higher than commercial supercapacitors) while maintaining the typical supercapacitor power density ( $\sim 1000$  W/kg).

## **2. LITERATURE REVIEW**

### **2.1 Materials**

In the past few decades, nanomaterials have undergone a revolution as new and improved methods of manufacturing and increased research have resulted in many materials being much more readily available for use in research labs around the country. Many of these materials have very interesting and novel properties when they broadly fall into the category of a nanomaterial. It is widely accepted that a nanomaterial is any such material that has one or more characteristic length in the range of 1-100 nanometers. To further define these materials, a common classification involves describing the number of dimensions that are larger than the 1-100 nanometer range. 0-D refers to materials that have all three dimensions in the 1-100 nanometer range, 1-D materials have 1 dimension between 1 and 100 nanometers and so on up to 3-D materials. Many of these materials will be discussed in more length in subsequent sections as well as much more detailed discussions surrounding the materials that were used for this project.

#### **2.1.1 Carbon Based Materials**

Carbon based nanomaterials have been around since the 1980s and have attracted much attention due to the interesting properties and many different geometries that carbon nanomaterials can exhibit. Among these, many kinds of nanomaterials including carbon nanotubes, nanohorns, nanoribbons, graphene, graphite, diamond, fullerene, carbon/graphene dots, and many other different geometries that have been used and researched and are shown in Figure 2.1 below. These geometries each have very interesting and unique properties as the geometry on the nanoscale has a large influence on the function of the material. Within these broad carbon structures, the many ways of creating these materials also have considerable effect on the properties of these materials. These materials also can be functionalized with other chemicals or compounds to create even more unique and interesting materials such as adding functional groups that allow the bonding of other nanomaterials.

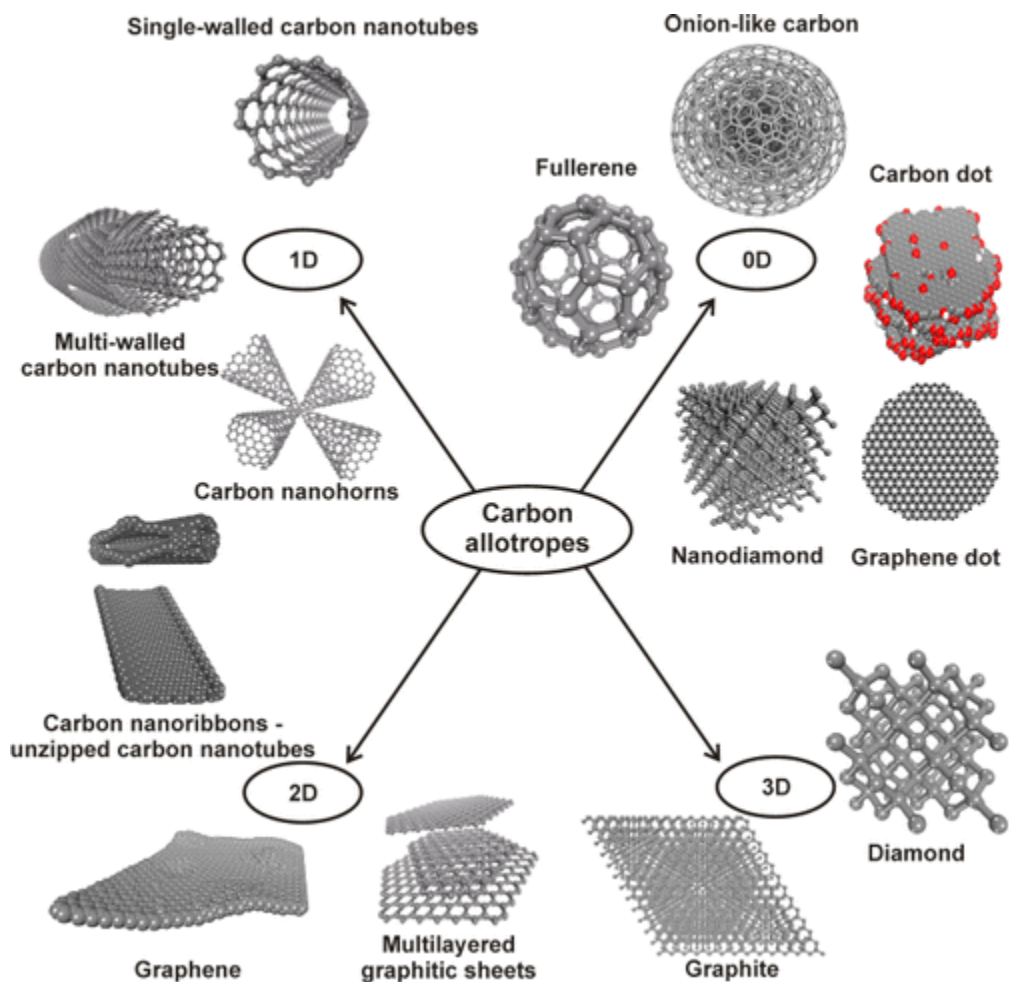


Figure 2.1. This figure shows the different allotropes of nanoscale carbon as well as their number of dimensions that are larger than the nanoscale. Image from [5], all rights and permissions inquiries should be directed towards ACS.

Carbon, because of its very flexible 4 valence electrons, has a number of different ways that it can bond together to make structures which are mainly based on the type of bonding that occurs between carbon atoms. When carbon is fully bonded, it can form many different orientations based on the type of bonding that is occurring with surrounding atoms. The type of bonding can radically shift the structure and properties of a material. Diamond is made of carbon and specifically carbon bonded in the  $sp^3$  hybridization which leads to diamond being a very strong material with very good hardness[6]. Graphite is also made of only carbon atoms just like diamond, but the bonds that graphite carbon atoms make are very different than the bonds of diamonds. Graphite has a  $sp^2$  hybridization meaning that it has three very strong bonds in the x-y plane with

one much weaker pi bond in the z direction. This makes a layered material, the bonding between the layers is very weak meaning that the individual layers of carbon atoms that make up graphite are very weak but the bonds between the intraplanar carbon atoms are very hard to disrupt or break.

It is precisely this structure of graphite that led to the discovery of graphene, which is made of only a single layer of carbon atoms that pi bond together to form graphite. Graphene is a 2-dimensional nanomaterial that has a very small, generally atomic, thickness but much larger length and width dimensions. Graphene is usually observed as a sheet and has been shown through much research to have several very interesting qualities including a very large surface area to volume ratio and excellent electrical conductivity[7], [8].

Graphene is a very interesting material in its own right, but the structures that can be created from rolling different sheets of graphene are potentially more interesting and have their own sets of unique properties. Carbon nanotubes are created by rolling graphene up into a tube-like structure which is capped on either end. The way in which the carbon nanotube is rolled directly impacts the material properties and characteristics of the material. Figure 2.2 below shows the different ways in which nanotubes can be rolled to create different structures. Generally, three basic types of nanotubes can be created by this rolling method: armchair, zigzag and chiral depending on the m and n vectors desired. The choice of the m and n vector can have a large impact of the structure and properties of the carbon nanotube and so it is important to consider this rolling method when considering the type of nanotube that is desired to be used in the project.

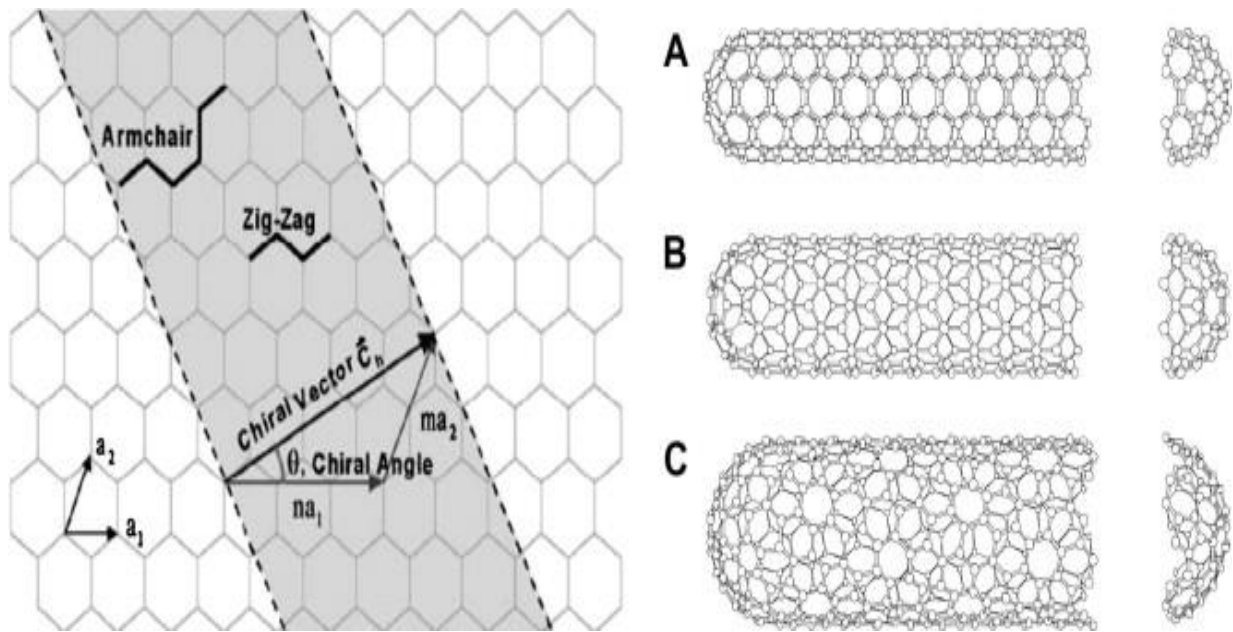


Figure 2.2. This illustrates the different methods by which graphene can be rolled to create carbon nanotubes with the three structural types of carbon nanotube (armchair, zigzag, and chiral) on display as well as A, B, and C, respectively. Image from [9] rights and permissions granted from Elsevier who should be contacted for all future rights or permissions inquiries.

Besides the crystal structure, another factor that can determine the geometry of carbon nanotubes is the number of walls that makes a single structure. Tubes can be either single walled (SWCNT) or multi-walled (MWCNT). A SWCNT is a single row of graphene that is rolled to make a singular carbon nanotube. MWCNT can be created using one of two methods, one is called the scroll method and involves rolling a single graphene sheet several times on top of itself to form a structure that looks similar to a scroll. The other method, the Russian doll method, places multiple sheets of graphene on top of one another and then rolls them all to create a multi-walled structure as a set of concentric tubes. Table 2.1 below summarizes some of the differences between SWCNTs and MWCNTs both in their structure and properties.

Table 2.1 Comparison of the properties of SWCNTs and MWCNTs. Reused from [6] N. Saifuddin et. al

SWCNT	MWCNT
Single layer of graphene.	Multiple layers of graphene
Catalyst is required for synthesis.	Can be produced without catalyst.
Bulk synthesis is difficult as it requires proper control overgrowth and atmospheric condition.	Bulk synthesis is easy.
Not fully dispersed, and form bundled structures.	Homogeneously dispersed with no apparent bundled formation.
Resistivity usually in the range of $10^{-4}$ – $10^{-3} \Omega \cdot m$ .	Resistivity usually in the range of $1.8 \times 10^{-5}$ – $6.1 \times 10^{-5} \Omega \cdot m$
Purity is poor. Typical SWCNT content in as-prepared samples by chemical vapor deposition (CVD) method is about 30–50 wt%. However high purity up to 80% has been reported by using arc discharge synthesis method.	Purity is high. Typical MWCNT content in as-prepared samples by CVD method is about 35–90 wt%.
A chance of defect is more during functionalization.	A chance of defect is less especially when synthesized by arc-discharged method.
Characterization and evaluation are easy.	It has very complex structure
It can be easily twisted and are more pliable.	It cannot be easily twisted.

The properties of carbon nanotubes vary quite substantially with both crystal structure and number of walls. Generally, one of the strengths of carbon nanotubes is their incredible length to diameter ratio which can be larger than one million with a diameter often in the range of 1-3 nanometers for SWCNTs and several nanometers more for MWCNTs with the outermost diameter often being between 2 and 100 nanometers. This results in a very large surface area to volume ratio which is optimal for energy storage devices like supercapacitors. Carbon nanotubes have also been shown to have a very good electrical conductivity (similar to that of a conductor like copper) and a band gap that is largely dependent on the diameter of the nanotube being observed but often is between 0.18 and 1.8 eV [6]. The carbon nanotube structure is also very strong, having a Young's

Modulus of around 1 TPa [8]. Additionally, the tensile strength is very good, measuring in the GPa range consistently and being many times stronger, and lighter, than steel [10].

### **2.1.2 Metal Organic Frameworks**

The term metal organic framework is a very general description used to refer to a family of materials that are composed of both metal ions and organic ligands the structure of which is shown below in Figure 2.3. These materials are highly tunable and very modular under the correct conditions and so make very good nanomaterials to work with in a variety of applications including energy storage, desalination, and gas storage. The specific characteristics of metal organic frameworks that make them a material that has attracted a great deal of research interest includes their relatively large surface area, ability to form unique shapes and structures, tunable porosity and pore size, and surface functionality by adding a variety of different constituents that can change the surface chemistry in advantageous ways. Like many different nanomaterials, these properties are tunable primarily from the preparations procedures that are used to create the material.

Metal organic frameworks are primarily created by using one of two general approaches: either a top-down or bottom-up approach. A top-down approach involves breaking the interlayer forces of a bulk metal organic framework to create numerous few layered materials, this is primarily done through using either physical or chemical exfoliation [11]. Both preparation methods can generate metal organic frameworks, however, chemical exfoliation techniques are largely preferred in research applications due to better control of both structural uniformity and yield [12] [13]. The other approach to generating metal organic frameworks is the bottom-up approach. This approach, instead of exfoliating from a bulk crystal, grows the crystal itself using the metal ions and ligands that make up the metal organic framework as bases and then controlling the growth of the crystal using methods such as ultrasound synthesis [14].

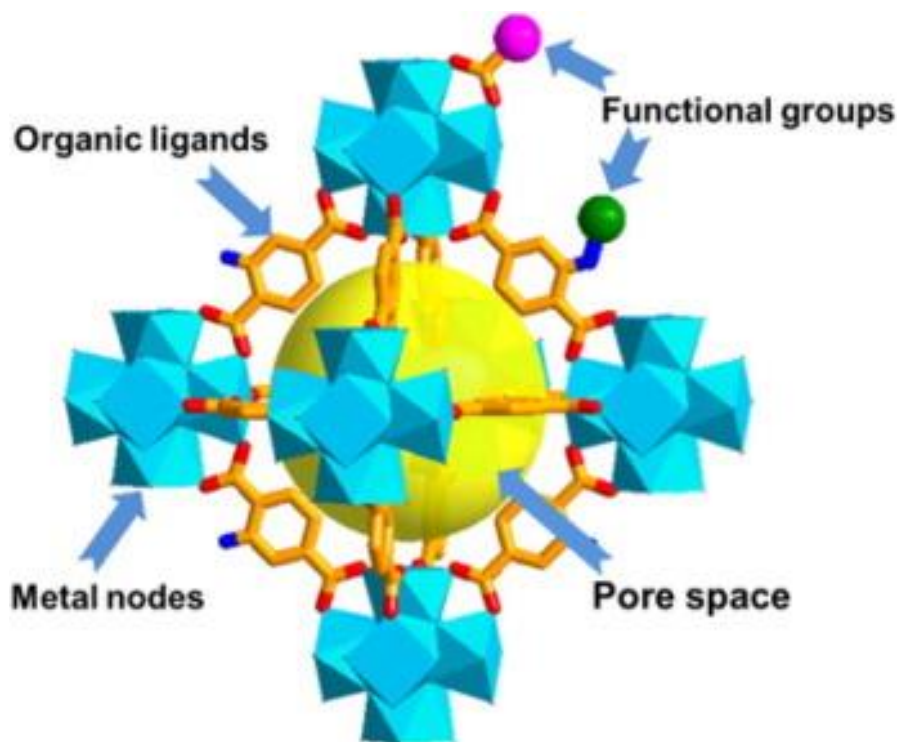


Figure 2.3. Image of the structure of a metal organic framework. Note the bonding between the organic ligands and metal nodes which make the characteristic structure. Used with permission from [15] with all rights and permissions held by Elsevier

Generally, there are an incredible number of discovered metal organic frameworks, with many of them being discovered recently as it is an area with much research interest[16]. A kind of MOF that is of distinction, and often as a result is named ZIF-x instead of MOF-x, is the zeolitic imidazole framework (ZIF)[17]. ZIF metal organic frameworks are highly stable structures with very high specific surface area. ZIF is structurally very similar to aluminosilicate zeolites, containing imidazole linkers connecting metal zinc ions [18]. ZIF also has the ability to be functionalized with several different working groups which can allow it to bond to a variety of other materials, including a sulfide group which will be of practical use later in this thesis.

### 2.1.3 Transition Metal Dichalcogenides

Transition metal dichalcogenides are another type of two-dimensional material that has attracted a lot of research attention lately. The name transition metal dichalcogenide is very self-descriptive and refers to any transition metal bonded to any 2 chalcogenide (Column 16 of the

periodic table) atoms. However, of particular interest in nanomaterials are the transition metals of column 4 through six that, when bonded with sulfides, form a layered structure that is very similar to that of graphene, which was discussed earlier in section 2.1.1, having very strong interlayer covalent bonds and very weak intralayer van der Waals bonds[19]. This creates a structure that is similar to graphene with individual layers that can be easily separated to reveal very interesting two-dimensional layers which have quite interesting properties, many of them of potential use in creating better energy storage devices such as lithium ion batteries [20].

The properties of transition metal dichalcogenides are very similar to other nanomaterials discussed in that they have a very high surface area to volume ratio making them ideal for capacitive energy storage. Additionally, these materials have a substantial energy bandgap as well as a number of gaps that could store positive or negative charge in energy storage mechanisms[21], [22]. The downside of these exciting materials is largely their poor conductivity which could limit their applicability in energy storage [23]. However, these materials have been shown to be combined through sulfur bonding with other materials to form structures that can overcome these individual weaknesses [24], [25]. Additionally, like many other nanomaterials, these properties are thickness and layer number specific [26].

Like the other nanomaterials mentioned, structure influences many of the properties of transition metal chalcogenides. There are three general bonding structures of these materials which is also coincidentally how many of these compounds are named. The three types of bonding that can occur are 2-H, 1-T, and 3R with each referring to the way that the layers of transition metal dichalcogenide are stacked onto one another and shown in Figure 2.4 below. Of these, 2-H is the most common orientation, occurring in naturally produced transition metal dichalcogenides, while 3-R is the least common naturally and occurs mostly in synthetically created materials. The letters T, H, and R refer to the type of symmetry that the crystalline structures have: Triagonal, Hexagonal, and rhombohedral respectively [25].

A specific type of transition metal dichalcogenide that shows promise as an energy storage material is molybdenum disulfide ( $\text{MoS}_2$ ) which like all transition dichalcogenides has a very large surface area to volume ratio and additionally shows a very large interlayer spacing which makes it very easy to separate layers to form a nanomaterial of very small thickness.  $\text{MoS}_2$  also has an advantage of being a very prevalent material that can easily be found in large quantities.

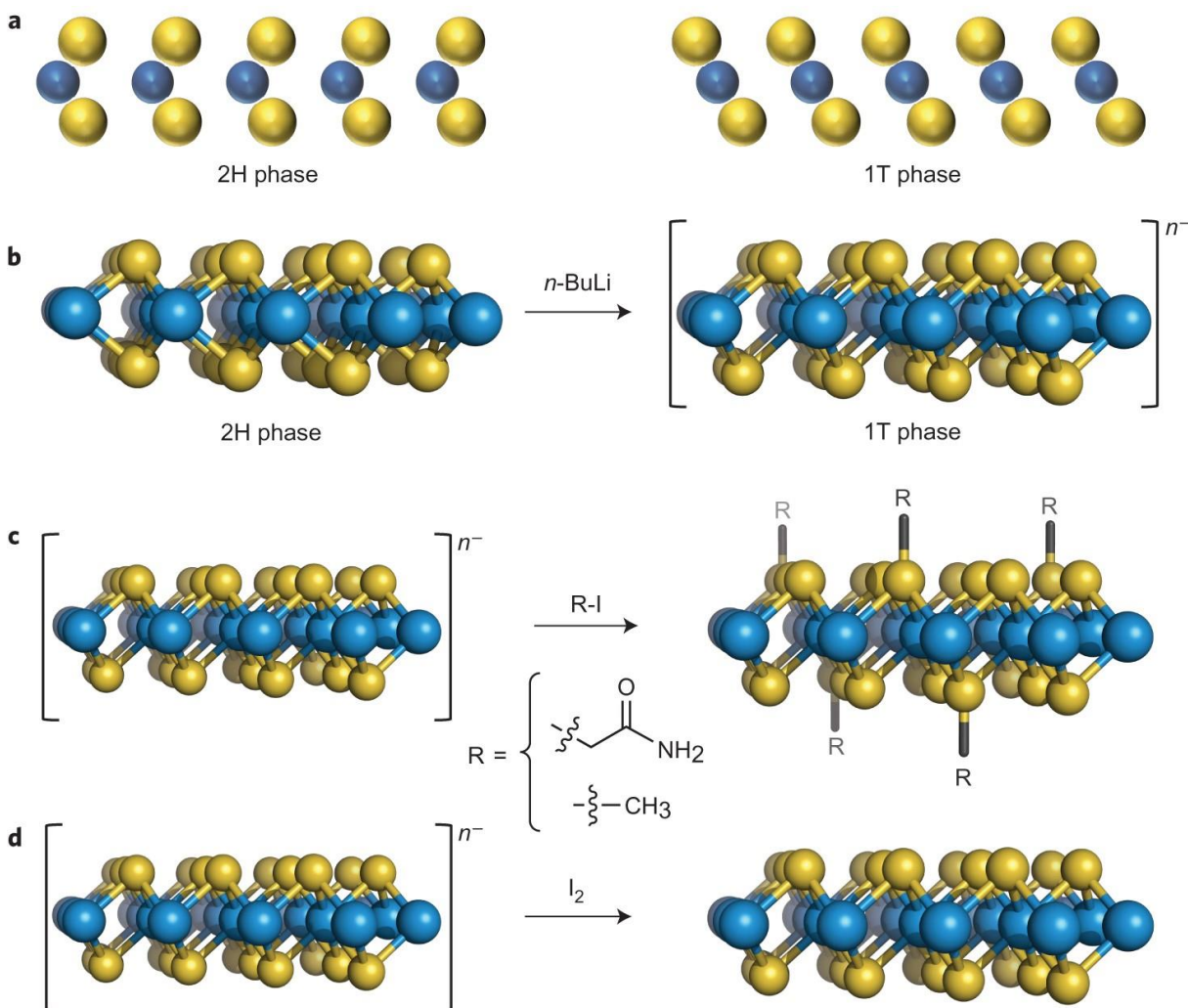


Figure 2.4. Demonstration of the structure and bonding of MoS<sub>2</sub> and other transition metal dichalcogenides with both crystalline structures, 2H and 1T, shown. Figure taken from [27] with rights and permissions granted by Springer Nature who owns the copyright of the material.

## 2.2 Energy Storage Devices

### 2.2.1 Electrochemical Energy Storage Technologies

Electrochemical energy storage devices are defined in this introduction as any method of energy storage that has a storage mechanism involving the storage of energy in some chemical form. This general definition encompasses a wide range of storage technologies from capacitors to batteries. Generally, many of these electrochemical energy storage techniques have a very similar setup, and the materials and charge characteristics change the performance of the cell. Most of these devices are composed of two current collectors, two electrodes, one or two electrolytes

and a separator that creates two separate cells (although this is not always necessary for some form of electrochemical storage). This general outline is shown below in Figure 2.5.

The purpose of the current collector is to act as a conductor between the electrode and the external device that is using the energy storage. This may seem trivial, but the choice of current collector greatly affects the performance of the cell by changing the allowable voltage range, by affecting the electrolyte performance by potential corrosion, and by potentially increasing the surface area of the device through a collector such as nickel foam. The electrodes are the general working material of the device. These are the part of the system that most directly influence the type and result of electrochemical energy storage and can be made from a wide array of materials to alter the performance of the device. The electrolyte can be either a fluid or organic solid and has the purpose of facilitating some chemical reaction between the two electrodes whether that is an oxidation in the case of a battery or simple negative and positive ion movements in the case of a supercapacitor. The electrolyte choice also plays a large role in the selection of the voltage window and the stability of the cell and so its selection is very important. Finally, a separator can be used in electrochemical cells to allow for charge transport but to prevent the passage of larger ions such as larger ions from the oxidation reaction that could foul the other electrode. Separators are primarily used in batteries or in supercapacitor applications that have two different electrolytes.

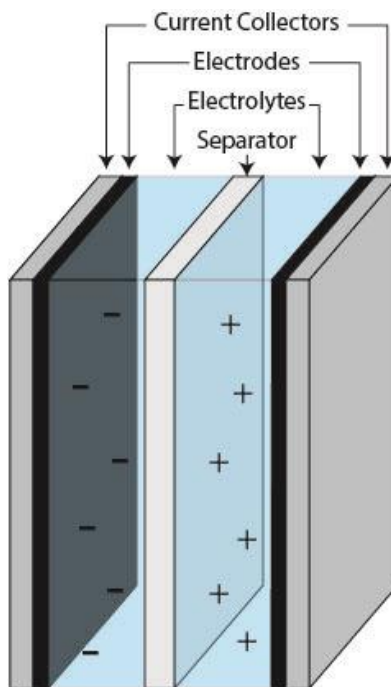


Figure 2.5. Schematic of a typical electrochemical energy storage system.

The measure of performance of these storage devices that is often compared when evaluating them is the energy and power density (or the specific energy and specific power). Capacitors have by far the highest power density and batteries have the most energy density, while supercapacitors, pseudocapacitors and all other combinations of the above falling somewhere between the performance of the two devices. The Ragone chart below shows each of these different electrochemical devices plotted on axis of energy and power density and is used to compare the devices.

Now that we have established the different types of electrochemical storage, we will discuss each in more detail in the coming sections including the theory, history, and modern research on the battery, supercapacitor, and hybrid/asymmetric devices.

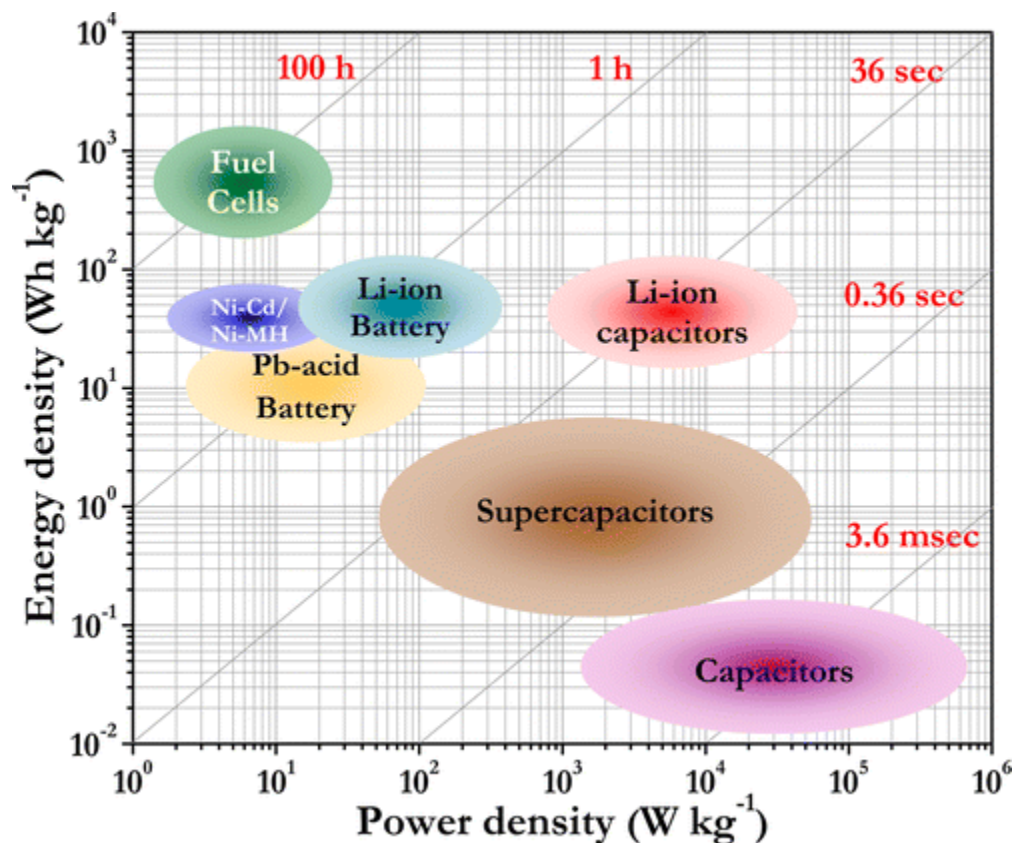


Figure 2.6. Ragone chart depicting the specific power and specific energy of various popular electrochemical energy storage devices. Notice that the values of the supercapacitors typically stretch from a specific power of between 100 and 30000 W/kg and energy density ranging from 0.1 to 8 Whr/kg. This figure is taken from [28] image used with the rights and permissions from ACS publishing.

## ***Battery***

### *History*

The history of the battery dates to the early 1800's when a scientist by the name of volta created the first primary battery cell. The first battery would be almost unrecognizable by the standards of batteries today and was a very simple design of alternating zinc and copper plates separated by cardboard in a brine (salt and water) solution. John Frederic Daniel then created the next iteration of the battery in 1836 by using two different electrolytes. The rechargeable battery was not invented until 1859 which was also the first lead acid battery. This led to a host of other rechargeable batteries being created and researched in the late 1800's into the early 1900's.

Generally, the next big wave of battery research came in the 1970's to 1980's. During this time, the lithium-ion battery and the Nickel cadmium battery entered the battery market and became the subject of a significant amount of research.

### *Theory*

Batteries on the most basic level, store energy in a chemical reaction which oftentimes, though not always, is reversible. If the chemical reaction is reversible, it is considered a rechargeable battery and can be used to store energy more than once. On the contrary, primary batteries have energy stored in irreversible chemical reactions which are completely depleted upon use. Whether they are primary or secondary batteries, both kinds of battery implement a faradic process which is very similar to the redox reactions that are popular in chemistry.

To begin, it would be helpful to more accurately define the parts of a battery cell. Referencing the diagram below (Figure 2.7), the two electrodes in a battery cell are referred to as the anode and cathode referring to the reactions that occur on these electrodes while discharging. The more positive electrode during discharging is referred to the cathode and undergoes reduction while the more negative anode undergoes oxidation and is called the anode. Sometimes, the cathode and anode will have the same electrolyte and sometimes the electrolyte will differ. When this electrolyte differs, it is referred to as the anolyte and the catholyte for the electrolyte of the anode and cathode. Generally, organic solid electrolytes perform much better than aqueous electrolytes due to the higher voltage window that they can operate at. The current collectors for the anode and cathode can be the same or different but they both must be chemically and

electrochemically inert at the voltages that the cell is operating at. Additionally, the separator should be either porous or ion conducting depending on whether there is a single electrolyte or multiple electrolytes.

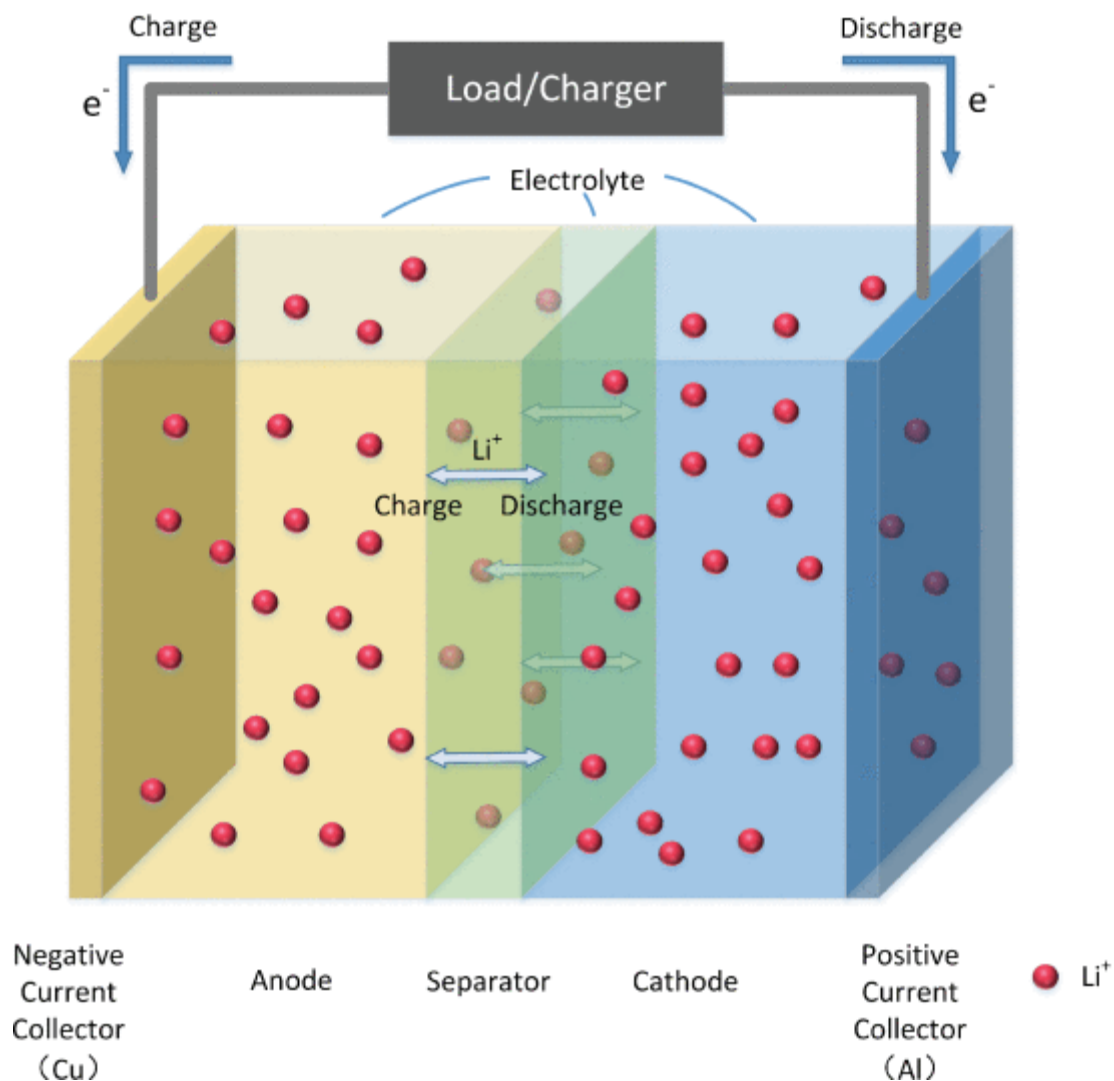


Figure 2.7. Schematic of a typical electrochemical battery cell. Note that the direction of the ion flux varies depending on whether the device is charging or discharging. Figure reproduced from [29] written by Zhang et al who own the copyright on the material and hosted by IEEE

The method by which batteries store energy is a Faradaic reaction. A faradaic reaction is very similar in mechanism to a redox reaction in chemistry. During discharging, the anode is undergoing oxidation (decreasing its potential) while the cathode is undergoing reduction (increasing in potential). This is the same as redox reactions, except that in faradaic reactions, charge may be added or withdrawn from the attached external circuit while during chemical redox

reactions electrons are always transferred from the electrode under reduction to the electrode undergoing oxidation.

The theoretical amount of energy that can be stored in a battery at any time can be predicted using the Gibbs free energy using the following correlations:

$$\Delta G = \Delta H - T\Delta S \quad \text{Eq 2.1}$$

and

$$\Delta G^0 = \Delta G_{products}^0 = \Delta G_{reactants}^0 \quad \text{Eq 2.2}$$

This change in Gibbs free energy can further be used to calculate a theoretical energy of any battery material and these are readily available in the literature but predominantly, in terms of specific energy, lithium is one of the highest performing materials [30].

### *Modern Research*

Today, much of the research on batteries involves trying to make batteries lighter (by achieving a higher specific or gravimetric energy) and with higher total energy density. Much of the goals of research today, to come out with the next generation of lithium-ion batteries focuses on moving batteries towards storing an order of magnitude such that they can compete with fossil fuels in terms of energy density and specific energy. Carbon and methane, the basis for most fossil fuels, have a theoretical energy of approximately -9.11 and -17.06 kWh/kg of energy [4] and even the highest theoretical energy that we can achieve with battery technologies with a lithium-oxygen reaction can only reach a limit of around -5.22 kWh/kg which is on the same order of magnitude as carbon and methane but still much lower meaning that a great deal of research should go into making these materials more efficient to approach the energy storage of carbon and methane.

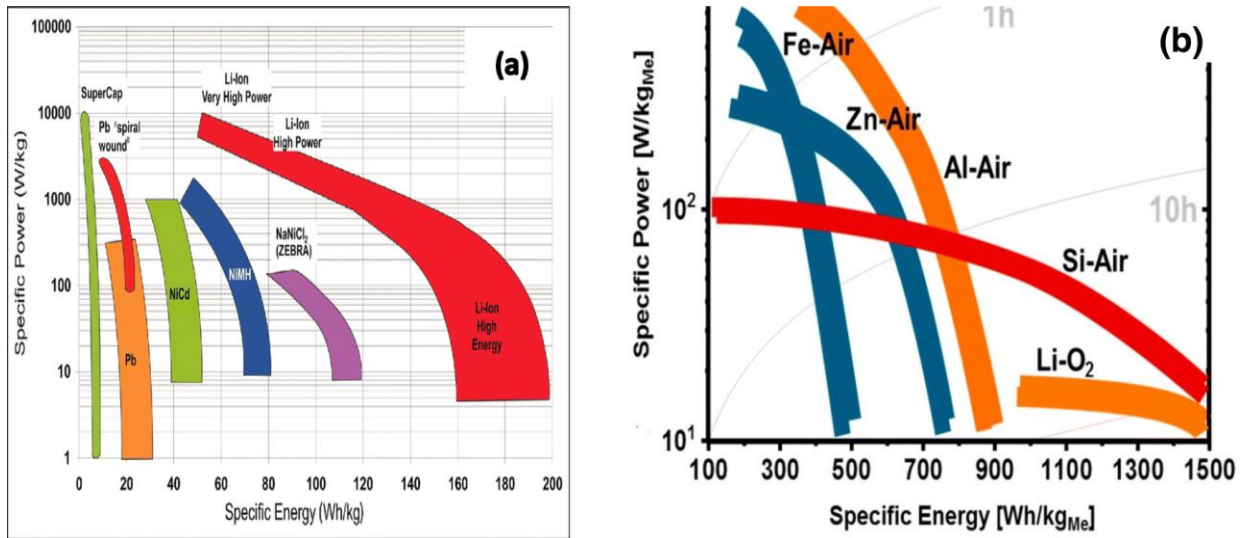


Figure 2.8. Ragone chart demonstrating the specific energy and power of common types of batteries as well as popular battery research technologies such as metal air batteries. Image taken from [31] with rights and permissions granted by Springer Nature who should be contacted regarding further uses of the copyright.

Currently, some popular kinds of batteries in research in rechargeable batteries are lithium-ion, sodium-ion, and lithium-sulfur. Each comes with a unique set of advantages and challenges that are a focus of much research attention now. A Ragone chart showing the energy and power density of many battery materials of recent interest are show on Figure 2.8 above.

## ***Supercapacitor***

### *History*

The history of the modern supercapacitor begins in 1879 with the prediction of the capacitive performance of the electrolyte/solid double layer, but the concept was not realized until nearly a century later when the carbon-based capacitors were first proposed and created by the General Electric Corporation. This device did not become commercialized until 1969, when the first electronic double layer capacitor was created from porous carbon and a tetra alkyl ammonium electrolyte. Up until 1978, the device had been referred to as an electrostatic double layer capacitor, but the NEC company marketed the device in 1978 as the first supercapacitor and the name has since stuck to refer to a number of different capacitor technologies including electrostatic double layer capacitors and pseudocapacitors [32]. There was not much development of this technology

until the 1990's when metal oxides began to be used and showed promise to have energy density closer to that of a battery which sparked a round of increased research interest which has continued to present day. Currently, supercapacitors are being researched for their high energy and power density and have applications in the electric car market, power grid regulating, and other forms of energy storage and transportation.

### *Theory*

Supercapacitors, similarly, to batteries, store energy in the form of electrochemical reactions. The primary difference between the two technologies is that while batteries store energy within the chemical reactions themselves, supercapacitors store energy as surface charge in the electrolyte-electrode interface. There are many advantages and disadvantages to this approach when compared to batteries. Because the energy is not stored in a chemical reaction, the energy density and specific energy of supercapacitors will not ever be as high as it is in battery technologies. With this being said, supercapacitors have a much faster discharge time due to their charge storage mechanism, which allows them to have a much higher power density and specific power as well as a much longer lifecycle because there are not as many irreversibilities in surface charge storage as there are in reversible chemical reactions.

The design of a supercapacitor cell is also very similar to that of a battery. Two electrodes are deposited on two current collectors, which are possibly separated by a separator, although for supercapacitors, separators are largely not used unless two different electrolytes are being used because unlike batteries there are no reaction byproducts that the separator is trying to prevent from mixing. Figure 2.9 below shows a typical schematic of a typical supercapacitor cell.

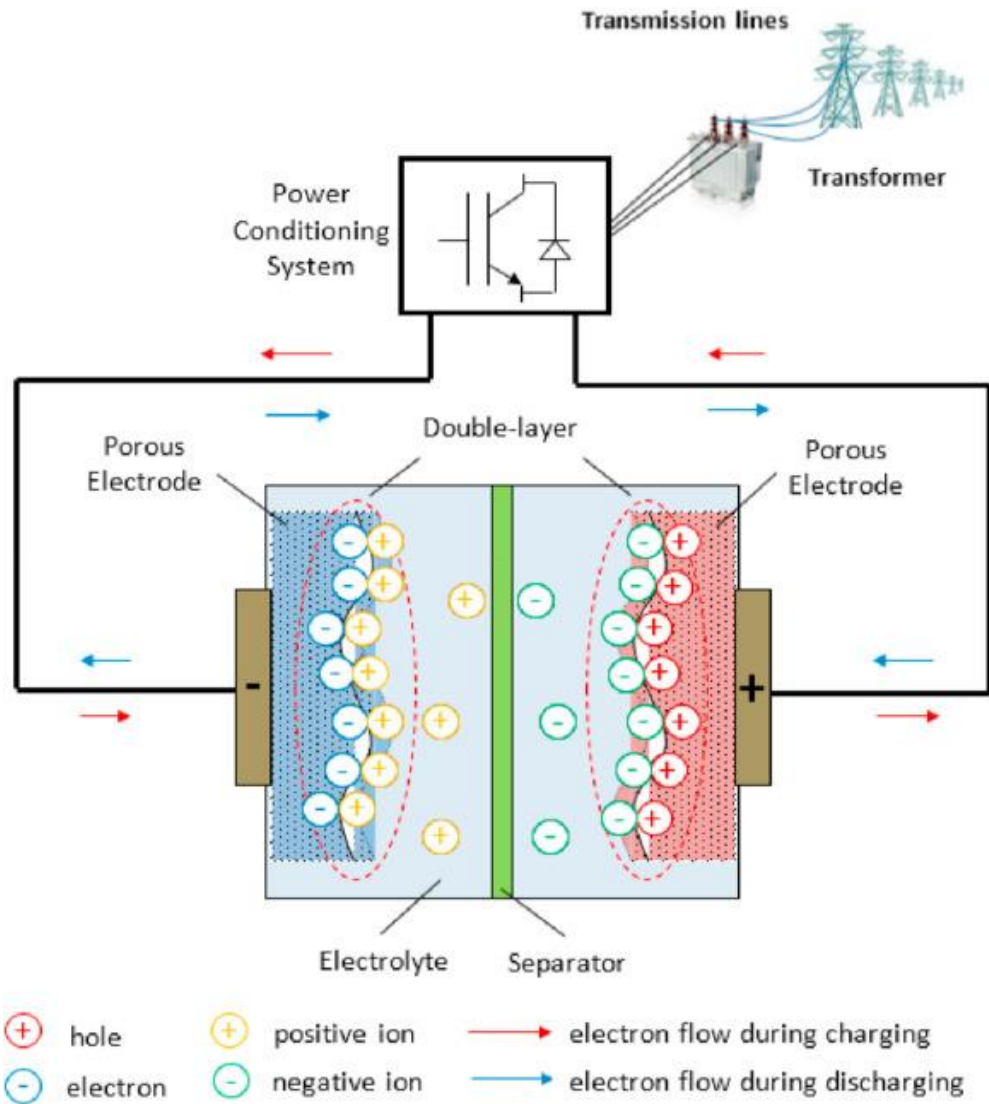


Figure 2.9. Image of the electrostatic double layer capacitor electrochemical cell showing all of the components necessary including the optional separator. This image is used from [33] with the right and permissions granted from Elsevier.

There are two general energy storage mechanisms that often get grouped together under the label of supercapacitor: pseudocapacitor and electrostatic double layer capacitor. The storage mechanisms are similar in that they both have very large capacitances and power densities, however, the capacitance and energy density of pseudocapacitors are usually slightly better because there are redox reactions that occur on the electrode surface which decreases the lifespan of the electrode but increases the energy and power density of the device generally when compared to electrostatic double layer capacitor performance.

To evaluate the performance of supercapacitors, it is important to look at both the fundamental laws that govern them and the equations used to derive test characteristics. We start with the fundamental equation for capacitance from parallel plate capacitors:

$$C = \frac{\epsilon_o \epsilon_r}{d} A \quad \text{Eq 2.3}$$

In this equation,  $\epsilon_o$  is the permittivity constant for a vacuum,  $\epsilon_r$  is the permittivity constant of the electrolyte separating the 2 electrodes,  $d$  is the Debye length, and  $A$  refers to the electrode contact area with the electrolyte. From this equation, it can be seen that the electrolyte choice and concentration are very important so that this equation can be maximized. Additionally, in the electrode material, a high surface area is important, as well as electrical conductivity and chemical stability within the electrolyte.

In determining the performance of real supercapacitor electrodes, it is often important to be able to determine the performance of an electrode from cyclic voltammetry or galvanostatic charge/discharge data. These equations have been derived and often used and accepted in literature:

$$C_{sp,cv} = \frac{1}{m\nu\Delta V} \int_0^{\frac{2\Delta V}{\nu}} IdV \quad \text{Eq 2.4}$$

The integral product is the area between the charging and discharging cyclic voltammetry curve,  $m$  is the electrode mass,  $\nu$  is the scan rate of the cyclic voltammetry program, and  $\Delta V$  is the voltage window of the experiment. Similarly, this equation can be solved for specific capacitance, substituting the area of the active material in for the mass to give an equation that follows:

$$C_{A,cv} = \frac{1}{A\nu\Delta V} \int_0^{\frac{2\Delta V}{\nu}} IdV \quad \text{Eq 2.5}$$

Similarly, the performance of a supercapacitor electrode can also be calculated using the galvanostatic charge-discharge curves using the following equation:

$$C_{sp,GCD} = \frac{I\Delta t}{m\Delta V} \quad \text{Eq 2.6}$$

Where  $I$  is the current,  $\Delta t$  is the discharge time of the experiment, and  $m$  and  $\Delta V$  are mass and voltage window as they were for the cyclic voltammetry data above. This equation, like the

equations for cyclic voltammetry, can also be adapted to an areal form by substituting area in for the mass of the substance, it is important to note that A is not the effective surface area of the nanomaterial, but is rather the size of the bulk electrode.

$$C_{A,GCD} = \frac{I\Delta t}{A\Delta V} \quad \text{Eq 2.7}$$

Outside of calculating the capacitance, energy, and power, the galvanostatic charge-discharge and cyclic voltammetry graphs also indicate the type of energy storage that is occurring, and the shape of the graph can be used as evidence to support the energy storage mechanism occurring at the electrode surface. Below, Figure 2.10 shows the difference in expected CV curve for an electrostatic double layer capacitor, pseudocapacitor, and battery. The cyclic voltammetry graphs of supercapacitor electrodes should appear as a rectangular or boxlike shape with a linear galvanostatic charge-discharge potential graphs. Batteries should have cyclic voltammetry graphs with redox peaks according to the chemical reaction that is taking place and additionally have plateaus on their charge-discharge graphs. Pseudocapacitors exhibit behaviors of both graphs, they exhibit a mostly rectangular cyclic voltammetry curve with some curvature or potential small redox peaks and additionally have mostly linear charge-discharge graphs with no detectable plateaus but also not completely linear in behavior.

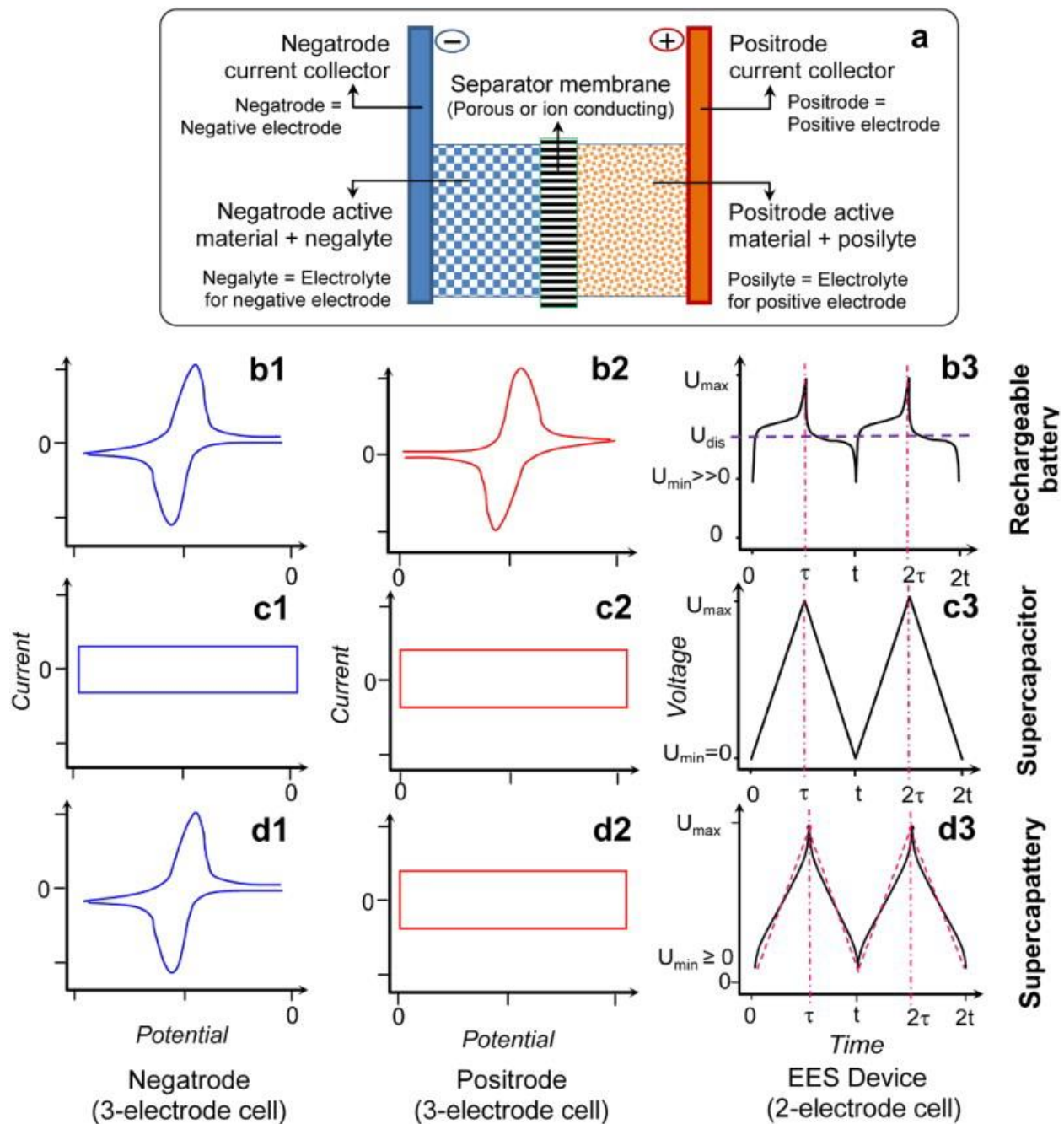


Figure 2.10. Cyclic voltammetry and galvanostatic charge-discharge graphs for three different energy storage devices: battery, supercapacitor, and a hybrid battery-supercapacitor system. Of special note is the shape of the different graphs, battery electrodes have oxidation peaks and have plateaus during charge-discharge testing, supercapacitors exhibit box-like cyclic voltammetry and linear charge-discharge graphs. Figure is used from [4] from George Chen hosted by Taylor and Francis.

Often when comparing the performances of supercapacitors, it is also helpful to compare the energy (either specific or density) and the power (once again specific or density) of electrodes. These equations are derived from experimental equations 2.4-2.7 above along with the classic definitions of energy and power for a capacitor:

$$E_{sp} = \frac{C_{sp}\Delta V^2}{2} \quad \text{Eq 2.8}$$

$$E_{den} = \frac{C_A\Delta V^2}{2} \quad \text{Eq 2.9}$$

$$P_{sp} = \frac{E_{sp}}{\Delta t} \quad \text{Eq 2.10}$$

$$P_{den} = \frac{E_{den}}{\Delta t} \quad \text{Eq 2.11}$$

When discussing the nanomaterials in an earlier section of the literature review, it was seen that many of these nanomaterials have had great potential properties that would make them good potential supercapacitor electrode materials including high surface area to volume ratio, good electrical conductivity, and the ability to be functionalized to bond together and form hybrid structures. As such, there has been much recent research on using and combining different nanomaterials to create higher performing supercapacitor electrodes. This has resulted in the energy density and power density of the supercapacitor making large increases in recent years as materials research has also improved. Some of the results of different nanomaterial combinations and their performances are included on the Table 2.2 below:

Table 2.2. Comparison of supercapacitor research being done on many different nanomaterials.

Material	Capacitance [F/g]	Electrolyte	Scan Rate [mv/s]	Current Density [A/g]	Reference
CNT-CZIF 2	324	6M KOH		0.5	[34, p. 8]
Graphene PTFE	116	5.5M KOH	40		[35]
Exfoliated graphene	117	1M H <sub>2</sub> SO <sub>4</sub>	100		[36]
Graphene Sphere	174	[BMIM]		8.4	[37]
CNT	61.2	TEABF <sub>4</sub>	1000		[38]
AWMWCNTs	83	NBF <sub>4</sub>	1		[39]
Carbon cloth/CNTs	225	0.5M Na <sub>2</sub> SO <sub>4</sub>		0.2	[40]
ZIF-69, activated carbon	168	0.5 M H <sub>2</sub> SO <sub>4</sub>	5		[41]
ZIF-8 Nanoporous Carbon	251	1M H <sub>2</sub> SO <sub>4</sub>	5		[42]
ZIF-8 Porous Carbon	219	1M H <sub>2</sub> SO <sub>4</sub>	5		[43]
ZIF-67 Carbon Nanotube	190	6M KOH		0.5	[44]
ZIF-8 MWCNT, Porous Carbon	326	1M H <sub>2</sub> SO <sub>4</sub>		1	[45]
ZIF-8/CNT, ZnO/CNT	250	1M Na <sub>2</sub> SO <sub>4</sub>		1	[46]
ZIF-67, Nanoporous Carbon	240	0.5M H <sub>2</sub> SO <sub>4</sub>	20		[47]
ZIF-7/glucose, porous carbon	228	6M KOH		0.1	[48]
ZIF-8, Hollow Carbon Spheres	280	6M KOH		1	[49]
ZIF-8, Nanoporous carbon	21	2M Net <sub>4</sub> BF <sub>4</sub>	10		[50]
WS <sub>2</sub> /rGo	350	1M Na <sub>2</sub> SO <sub>4</sub>	2		[51]
MoS <sub>2</sub> /rGo	265	1M HClO <sub>4</sub>	10		[52]
MoS <sub>2</sub> /MWCNT	452.7	1M Na <sub>2</sub> SO <sub>4</sub>		1	[53]
3D Graphene/MoS <sub>2</sub>	169.37	0.1M KOH		1	[54]
Porous Carbon/MoS <sub>2</sub>	210	3M KOH		1	[55]
Carbon Fiber cloth/WS <sub>2</sub>	399	1M KCl		1	[56]
MoS <sub>2</sub> -NiO	1080.6	6M KOH		1	[57]
MoS <sub>2</sub> -CoSe <sub>2</sub>	2577	6M KOH		1	[58]
MoS <sub>2</sub> /Bi <sub>2</sub> S <sub>3</sub>	1258	6M KOH		30	[59]
NiSe@MoSe <sub>2</sub>	223	2M KOH		1	[60]
3D tubular MoS <sub>2</sub> /Pani	552	1M H <sub>2</sub> SO <sub>4</sub>		0.5	[61]
MoS <sub>2</sub> /PPy	700	1M KCl	10		[62]

### *Hybrid/Asymmetrical Devices*

Hybrid devices are novel electrochemical storage devices that combine battery, pseudocapacitor and/or electrostatic double layer capacitor electrodes to combine the benefits of both batteries and supercapacitors while minimizing some of the weaknesses. This can lead to very interesting properties of energy storage systems with quite interesting characteristics. For example, a hybrid supercapacitor can be used to increase the effective operating voltage range of a supercapacitor electrode which significantly increases the energy density. The Supercapacitor electrode with a battery electrode can also increase drastically the power of the battery and additionally, outside of the performance boosts, can also positively affect the stability of the battery electrode. However, since the cell could potentially operate as more of a supercapacitor or a battery, the performance can be dominated by either the capacitive behavior or the battery redox behavior. This means that care must be placed into designing these systems to avoid damaging the structure of the electrode, such as keeping the lower potential higher than 0 to avoid lithiation on the carbon electrode [4]. Figure 2.11 shows the various charge-discharge graphs that can be produced by different hybrid electrochemical storage devices.

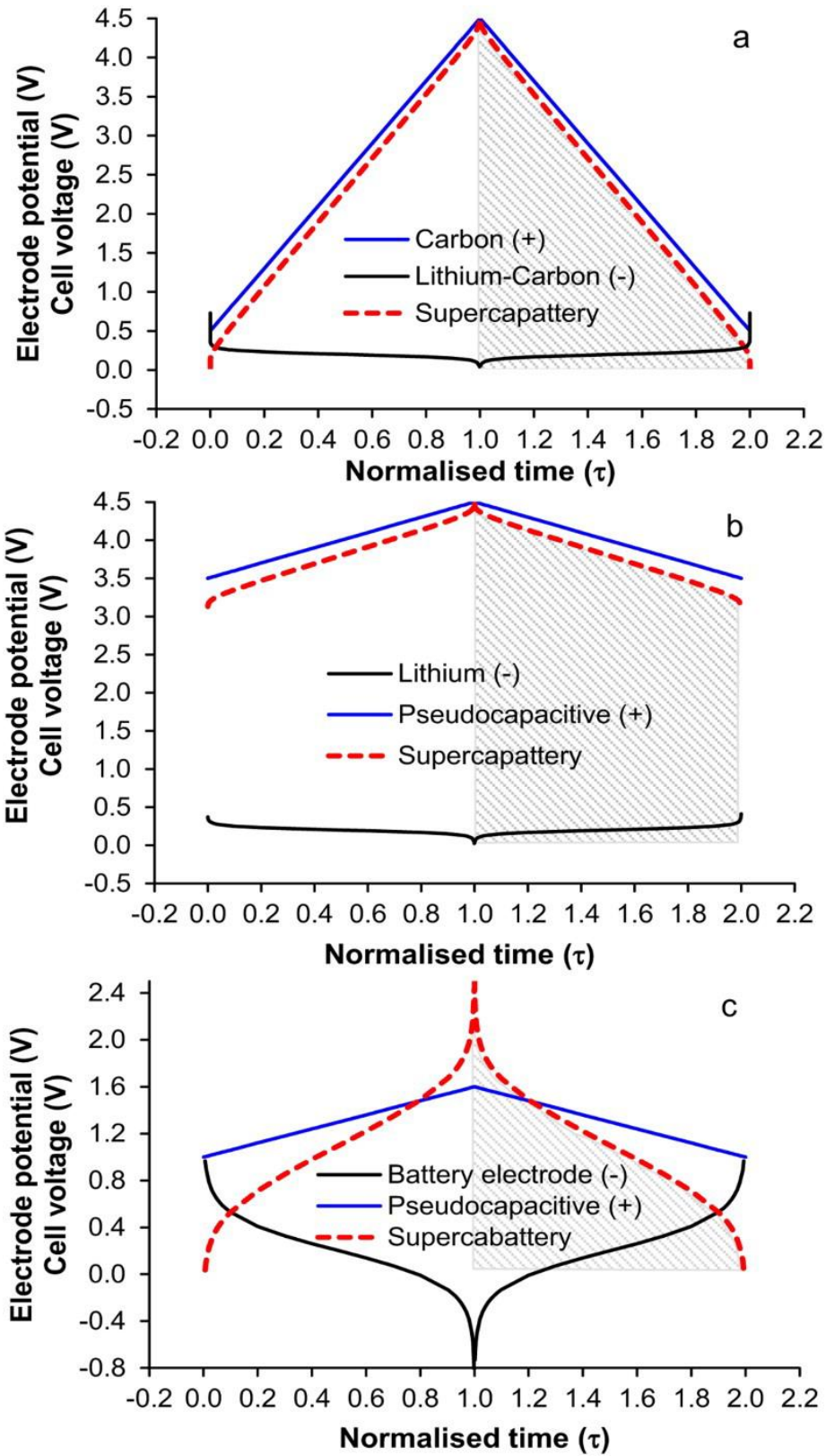


Figure 2.11. Comparison of charge-discharge performance of pseudocapacitor, supercapacitor, and battery electrodes. Figure taken from [4] from George Chen hosted by Taylor and Francis.

### 3. MATERIALS AND METHODS

After searching the literature and comparing different materials, it was decided that in order to make a research contribution to the field of energy storage, that an electrostatic supercapacitor electrode would be synthesized from three of the materials: carbon nanotubes, molybdenum disulfide and ZIF-8 which can be functionalized to have sulfur bonding sites on its surface in order to bond the  $\text{MoS}_2$  to the structure. With using this many different materials however, it became important to accurately prepare them in such a way that the bonding of all the different materials would work as intended. Additionally, this project sought to use a manufacturing method, that did not involve the high cost (in effort and material) steps that are normally utilized in electrode synthesis such as very high temperature calcification and binding electrolytes to create a slurry which must be deposited on a current collector at high pressure and temperature. Additionally, different concerns about the construction of the testing environment, as well as current collector and electrolyte choice, will be discussed in this section. Figure 3.1 provides a graphical overview of the synthesis process used for the project.

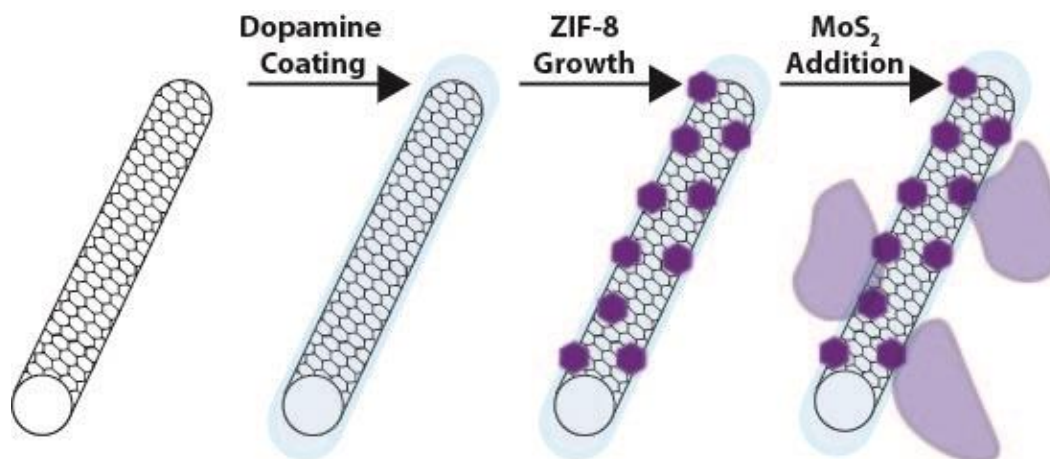


Figure 3.1 Overview of the material synthesis process. First a layer of polydopamine hydrochloride is applied to the carbon nanotubes. After that, ZIF-8 is bonded to the carbon nanotubes by bonding with the dopamine. Finally, few-layered  $\text{MoS}_2$  flakes are deposited onto the ZIF-8 via disulfide bonding.

### 3.1 Synthesis of CNT, ZIF-8, MoS<sub>2</sub> Framework

As mentioned above, to get the benefits of each of the individual nanomaterials, it was important to combine the materials in the correct way [63], [64]. The first step in this process is to create the carbon nanotube base that we will build the rest of the framework upon.

The first step in any carbon nanotube preparation procedure is to find a suitable way to disperse the carbon nanotubes in solute (because the nanotubes are normally sold in a powder form). To do this, there are many different options that can be pursued but generally techniques that are widely used fall under the broad category of mechanical and chemical techniques. Mechanical techniques include processes like ultrasonication, calendaring, ball milling, shear mixing, and extrusion. Of these choices, tip sonication is the most utilized method of CNT dispersion and is the simplest to use [9]. This method however comes with some disadvantages, namely that it can denature the carbon nanotubes if the nanotubes sonicate for too long a time. Therefore, care should be taken to keep the nanotubes cool by placing the sample in a water (or ice) bath while sonication occurs. This was the method used for the project, carbon nanotubes were sonicated for an hour to allow plenty of time for dispersion to occur without denaturing the carbon nanotubes.

An additional consideration for the dispersal is the fluid of dispersion. There are many different fluids that have been proposed for dispersion of carbon nanotubes. Among others, DMF (N-N-Dimethylformamide), ethanol, acetone, diethyl ether, PDDA, and methanol are some widely used solutes. The dispersed nanotubes in each of these different solutes will have slightly different properties due primarily to the different chemical structures and properties of each solute [64]. For example, DMF is very good for dispersing carbon nanotubes in microdroplets leading to bundles of carbon nanotubes being formed that look like small droplets [65].

The choice of fluid for this project was driven by another factor as well, ethanol has been reported to not only be a good fluid for carbon nanotube dispersion but it also, in the presence of water, can help mediate the polymerization of the carbon nanotubes via polydopamine hydrochloride (dopamine) which is integral to allowing the formation of ZIF on top of the carbon nanotubes [66]. This polymerization could be done in only water, but the presence of ethanol was found to slow down polymerization rate and thus make the coating more controllable and uniform in creation [67]. For the process to create a sample, 5mg of HiPCO carbon nanotubes (carbon nanotubes made from a high pressure carbon monoxide process) were dispersed in 20ml of ethanol

and 15 ml of deionized water via one hour of tip sonication similar to the preparation procedure seen in other literature involving the combination of carbon nanotubes and ZIF [34] [68]. 50mg dopamine was added to the resulting dispersed carbon nanotubes along with 10ml of tris 1x under constant stirring and allowed to react for two hours undisturbed. This created a coating on the nanotubes that allows for the addition of the Zif-8 molecules in the subsequent step.

After the carbon nanotubes had been sufficiently dispersed and coated in dopamine, the next step was to synthesize ZIF-8 on the new bonding sites created by the dopamine. DMF which was previously cited as a good solvent for dispersion of carbon nanotubes, has also been cited as a strong solvent for growing ZIF-8 [69]. To remove the ethanol and water that was previous being used as the solute for the carbon nanotube dopamine compound, centrifugation was performed at 15000RPM for 12 minutes which was found through experimentation to result in the best separation of the carbon nanotubes from the ethanol-water mixture. After the sonication, the resulting carbon nanotubes were redispersed in DMF by adding them to 20ml of DMF and tip sonicating the mixture for 30 minutes to fully redistribute. After the redistribution, the ZIF-8 was synthesized on the polydopamine coated carbon nanotubes by adding 1,2,4-triazole-3-triol (3-thiol) and zinc chloride (ZnCl) at a mass ration of 2:1 as reported previously in the literature [70]. The resulting mixture was transferred to a heating element (oven) and kept at a temperature of 120 degrees Celsius for 48 hours to allow the ZIF-8 to form and functionalize correctly. This process is illustrated in Figure 3.2 shown below.

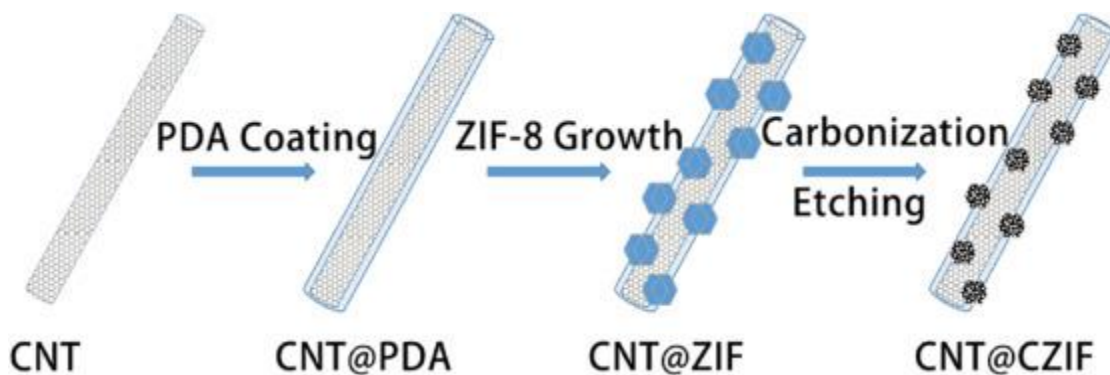


Figure 3.2. Process of synthesizing a carbon nanotube and ZIF-8 compound by using a polydopamine mediated process. Cited from [34] with rights and permissions granted by Elsevier publishing

After the ZIF-8 had fully formed on the carbon nanotubes over the 48 hours at constant heating, molybdenum disulfide was added to complete the framework that was being built. The

method for forming ZIF-8 that was previously reported was chosen because of the disulfide bonding that occurs in this variant of ZIF-8 that is created by mixing 3-thiol and zinc chloride, CPM-8S. This CPM-8S variant, because of its sulfide bonding, can form covalent bonds with molybdenum disulfide, bonding with the naturally occurring sulfur vacancies in the material[66]. Molybdenum disulfide can also be synthesized with additional sulfur bonds to create additional bonding opportunities to the nanotube-ZIF-8 framework which is something which could be pursued in further studies[71], [72]. To synthesize molybdenum disulfide, bulk molybdenum disulfide powder was dispersed in DMF via sonication for 1 hour at a 1:1 mg MoS<sub>2</sub> to ml DMF ratio and added to the mixture that had previously been reacting in the over at 120 degrees Celsius [72]–[74]. The dispersed molybdenum disulfide then bonds to the carbon nanotube-ZIF-8 compound via the disulfide bonding over the next 24 hours under 80-degree Celsius conditions[75].



Figure 3.3 Vacuum Filtration process used to remove solute from sample to deposit electrode material onto membrane.

After the solution was given significant time to react, the mixture needs to be filtered in order to isolate the framework from the solute. This is done by placing a membrane on a vacuum filtration system (shown in Figure 3.3) and filtering the mixture through the membrane to remove the DMF working fluid while leaving the main carbon nanotube-ZIF-8-MoS<sub>2</sub> structure intact. The disk was then rinsed with large amounts of ethanol and DI water to clean off any contaminants that may have been left by the synthesis steps outlined above. Finally, the membranes are also then heated at 110 degrees Celsius for at least 12 hours to further burn off contaminants and dry the sample in order to prepare it for electrochemical experiment, this disk then forms the electrode for testing the material using the electrochemistry testing that will be outlined in the next section.



Figure 3.4. Image of completed electrode deposited onto nickel foam using conductive epoxy.

Because the electrode preparation process is very different than many of the different electrode formation processes used in the literature, the difference is described in this section. Typically, the previous step of vacuum filtration is often replaced by a burning or calcification

process followed by rinsing steps to collect the working material and then mixed with a binder and conductive additive to create a homogenous slurry which is then pasted onto a current collector and pressed under heat to dry out. This procedure generates a very good electrode but requires a lot of heating and washing steps that have been replaced by the much quicker and less intense vacuum filtration in this project. The resulting electrode was then fastened to an electrode using a commercially available conductive epoxy. The resulting electrodes were then heated to cure the epoxy and then tested in the electrochemical testing bench and is shown in Figure 3.4 above,

### **3.2 Electrochemical Testing**

Electrochemical testing for this project took place on the test bench pictured below in Figure 3.5. Cyclic voltammetry was performed to evaluate the performance of the electrode using a potentiostat/galvanostat model 263A from Princeton Applied Research and additionally using the Electrochemistry Powersuite program also provided by Princeton Applied Research. To test a single electrode, a three-electrode cyclic voltammetry study may be conducted to measure the current through the electrode at a linearly changing voltage sweep. The three-electrode test is recommended to use over a two-electrode test for this application because of the increased stability that the reference electrode gives to the linear voltage change of the working sample.

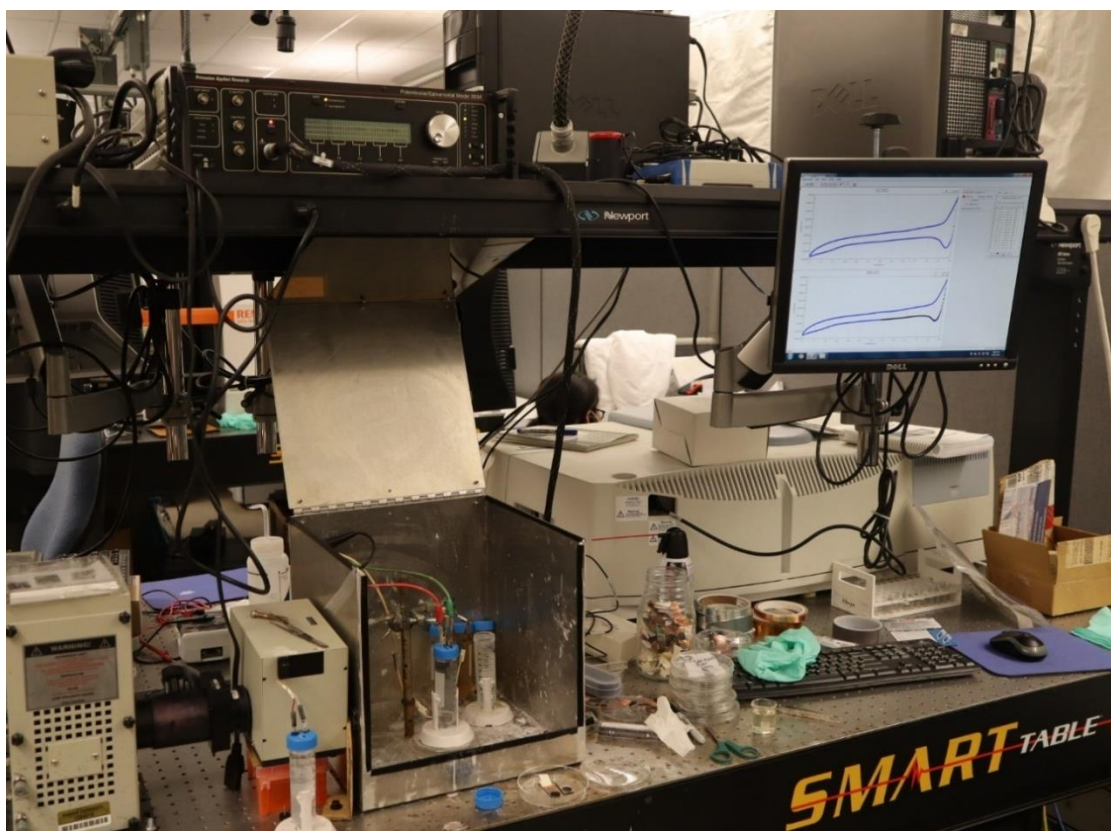


Figure 3.5. Image of electrochemistry testing bench



Figure 3.6. Image of 3 electrode electrochemical cyclic voltammetry test setup. The setup consisted of 1Ag/AgCl reference electrode, 1 platinum plate counter electrode, and the working electrode.

A 3-electrode cyclic voltammetry test consists of three main components: a reference electrode, a counter electrode, and the working electrode pictured above in Figure 3.6. The working electrode is the electrode disk that was created in the procedure above and deposited onto a nickel foam current collector using electrically conductive epoxy this will also be the material that is studied during the varying of the voltage. The counter electrode has the primary purpose of completing the circuit with the working electrode. As the voltage is varied across the working electrode, it will produce a current that must be accepted by the counter electrode to complete the circuit. The material for the counter electrode must be inert in the electrolyte of choice and ideally would have a high electrical conductivity. For this study, platinum plates were created for use as a counter electrode by depositing a thin layer of platinum metal on a glass slide by using chemical vapor deposition. Platinum was used due to its very high electrical conductivity and chemical inertness at the voltages and pH used for the experiment.

The additional electrode is called the reference electrode and has the primary purpose of supplying a reference potential to the system to regulate the potential applied to the working

electrode. The reference electrode does this by using one of several well-known materials with a well-known potential in a very well-defined electrolyte. For example, one common reference electrode is the Ag/AgCl electrode that is submersed in some concentration of KCl (usually 3-3.5 molar). The reference electrode shifts the potential of the system from absolute potential to the potential relative to the potential of the reference electrode which for the AgCl electrode is 0.197V. One common issue with reference electrodes is that, over time, the AgCl coating becomes completely oxidized which changes the potential of the system. This can be corrected for by bleaching the electrode by submersing the silver wire in bleach to restore the AgCl layer.

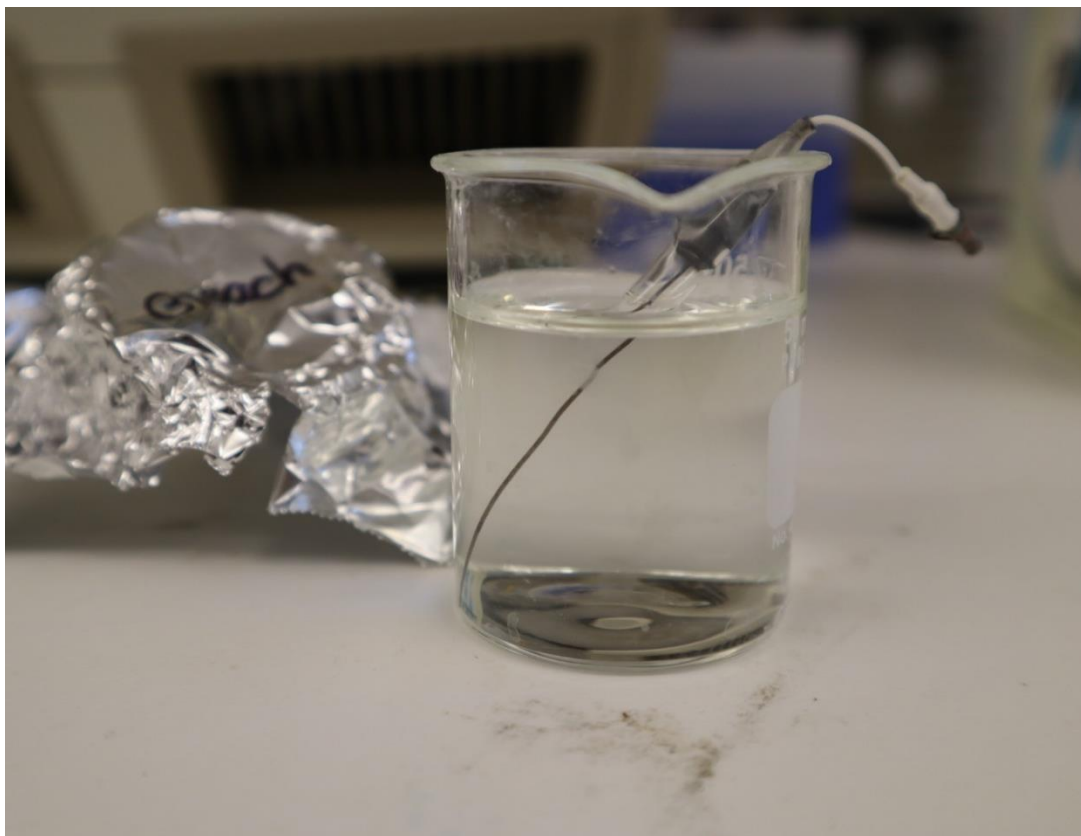


Figure 3.7. Bleaching process by which the thin layer of AgCl is restored to the outer surface of the silver wire in the Ag/AgCl electrode

To more accurately describe the cyclic voltammetry tests, the potential is varied at a constant rate (referred to as the scan rate of the test) and the system monitors the current that is being output by the working electrode. The upper and lower bounds of the scan are determined by the material. To determine this voltage window, several tests were run to determine where the peak shown in the graph occurs to set the upper bounds of the voltage window. After the voltage window was

determined for the material, each sample was run several times in the electrolyte of choice to determine the specific capacitance and specific energy and power as determined by the equations in the literature review section (equations 2.4-2.11).

A potential issue that occurs with the creation of these samples is sedimentation. Sedimentation is the process by which the sample settles at the bottom of the test tube and loses part of its dispersion. It was also found through testing that this sedimentation significantly affected the performance of the electrode and resulted in a weaker performing electrode shown in Figure 3.8 and Figure 3.9 below.

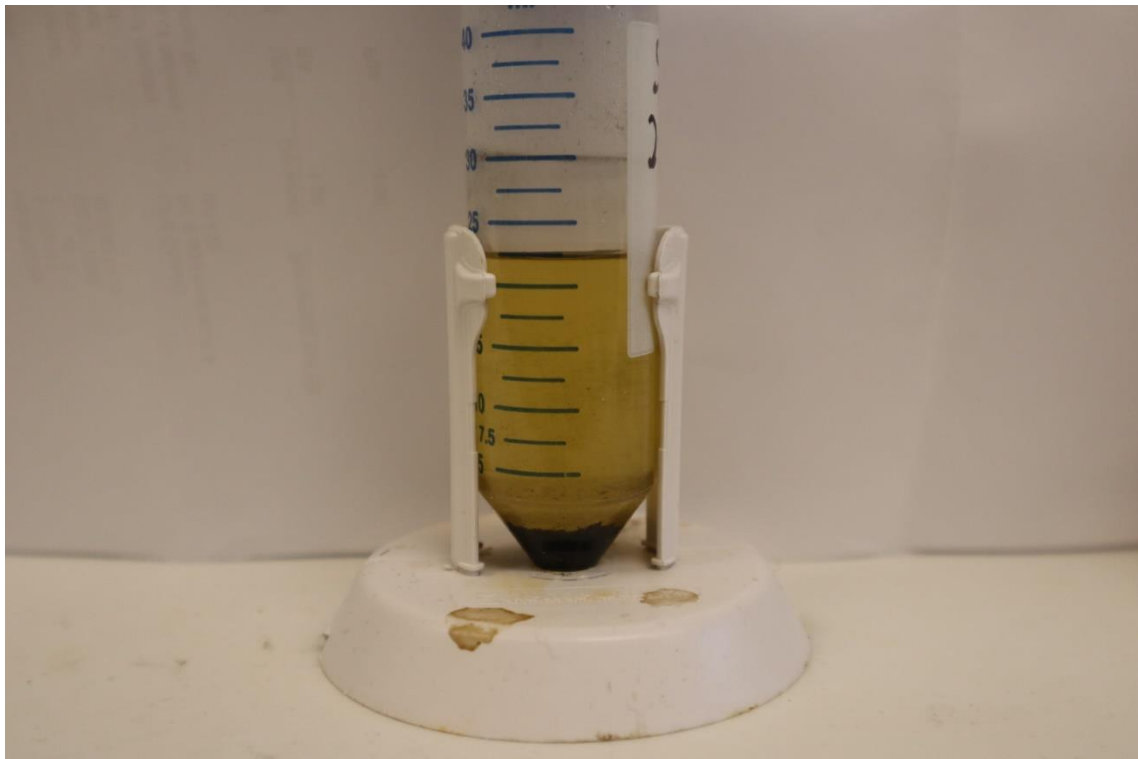


Figure 3.8. Picture of sample that had sat unused for a long time showing a large degree of sedimentation.

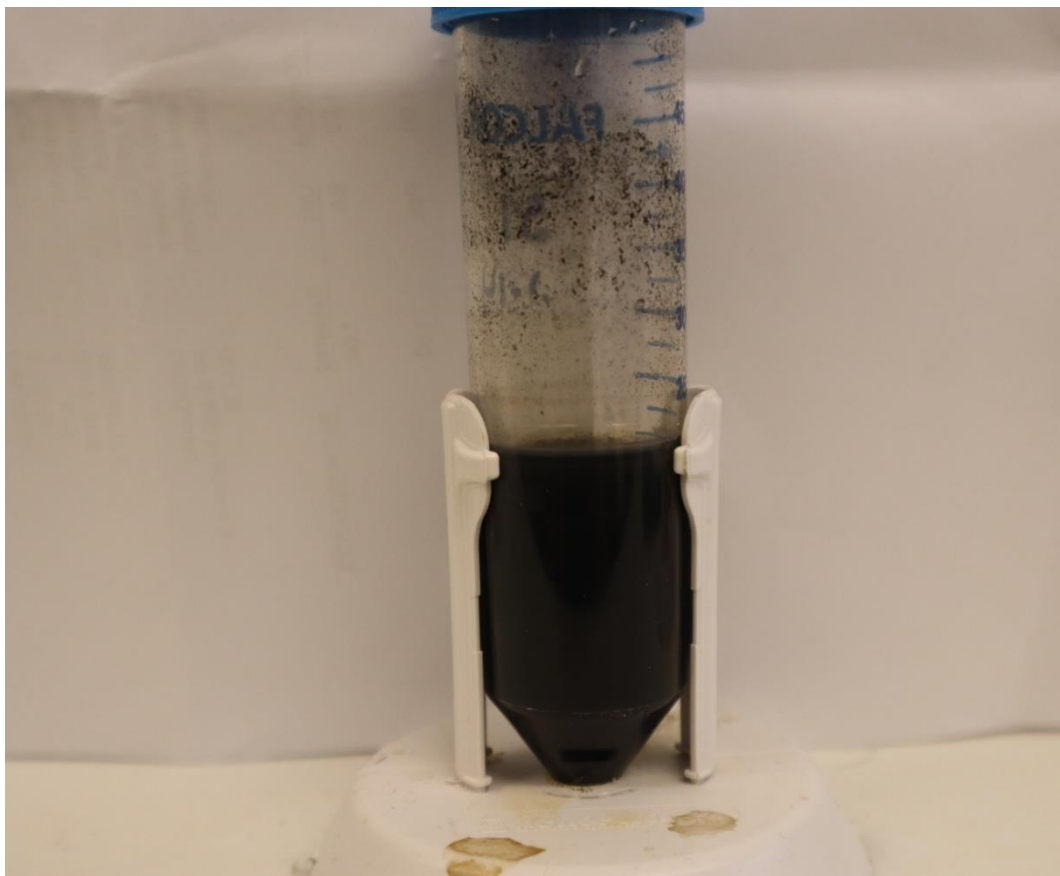


Figure 3.9. Image a sample shortly after being removed from the oven with a very well-dispersed consistency.

### 3.3 Choice of Current Collector

The choice of current collector can largely impact the results of the any cyclic voltammetry test. If a material is chosen that is not chemically inert, the current collector can corrode within the sample. The result of this corrosion is a steady decrease in the performance of the electrolyte and subsequently the working electrode[76]. This means that to design an optimum supercapacitor, care must be shown to select the correct electrolyte in order to prevent this corrosion from occurring. To prevent the corrosion, a Pourbaix diagram for each current collection material should be referenced as well as the pH of the material of interest. For example, copper tape was also posed as a current collector for this experiment, but it was found to corrode steadily in the electrolyte and so the current collector was switched to be nickel foam. A figure showing the samples on copper tape can be found below in Figure 3.10, they were also used as the conductive substrate for the SEM measurements that are in the results section.



Figure 3.10. Samples deposited onto copper tape that showed large degrees of corrosion.

As an example of how these diagrams can be of use, examine the following Pourbaix diagram for copper in Figure 3.11. From this figure, the experiment utilized an electrolyte of 6M KOH, we could calculate the pH of that system to be very high, around 14.77, which is a very strong, basic system. Reading the Pourbaix diagram of copper, it can be seen that at very basic pH levels, around the voltage window of 0 to -1.2, oxidation of copper occurs in the solution. This oxidation is a corrosion of the material and worsens the effectiveness of the electrolyte and the system. This is in line with what the literature predicts on this topic, that the corrosion of copper can quickly degrade the performance of a battery or a supercapacitor electrodes performance if allowed to oxidize [77].

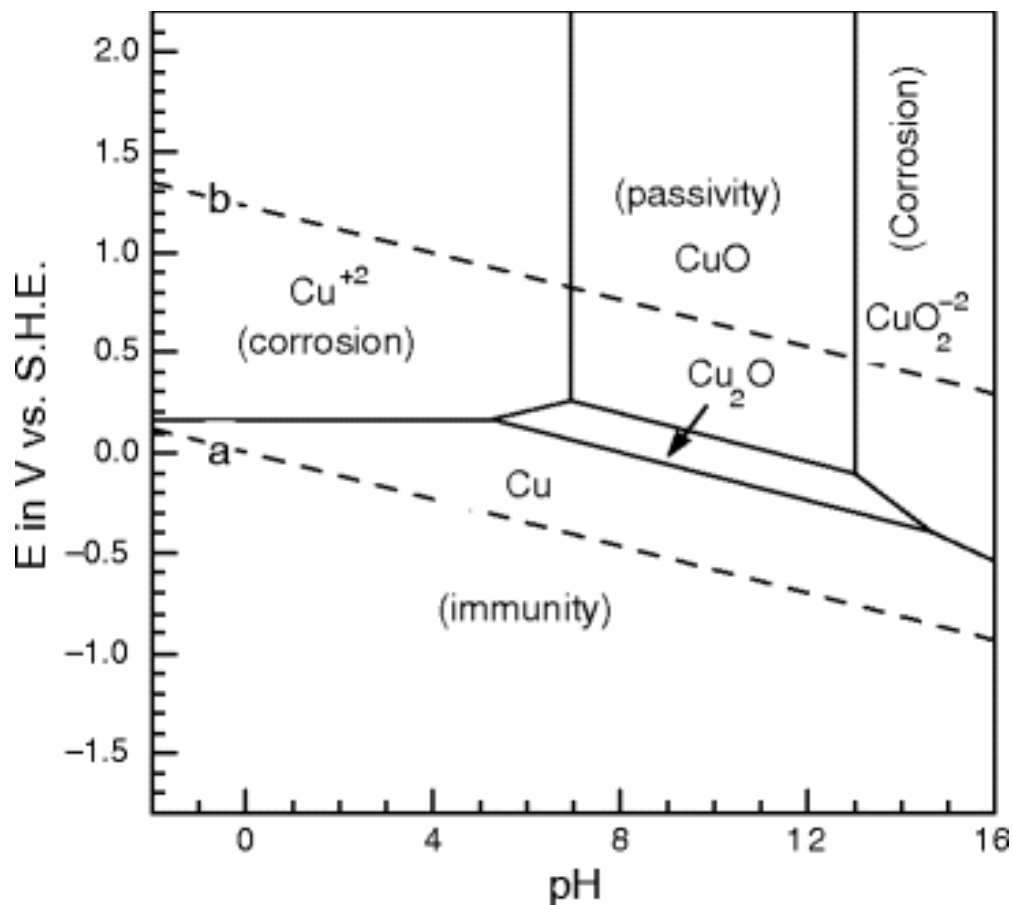


Figure 3.11. Pourbaix diagram of copper in aqueous solution (electrolyte) showing corrosive behavior at the pH of 6M KOH in water. Taken from [78] with permission from Springer Nature publishing.

In a conventional battery or supercapacitor, this may not necessarily be as large of a problem, because the electrolyte should theoretically never come into contact with the current collector however, due to the limits of the 3-electrode system, the electrolyte is in contact with the current collector and so can corrode the material. Below, in Figure 3.12, is an image of the corrosion observed in electrolyte for various stages of the copper tape being used as a current collector.

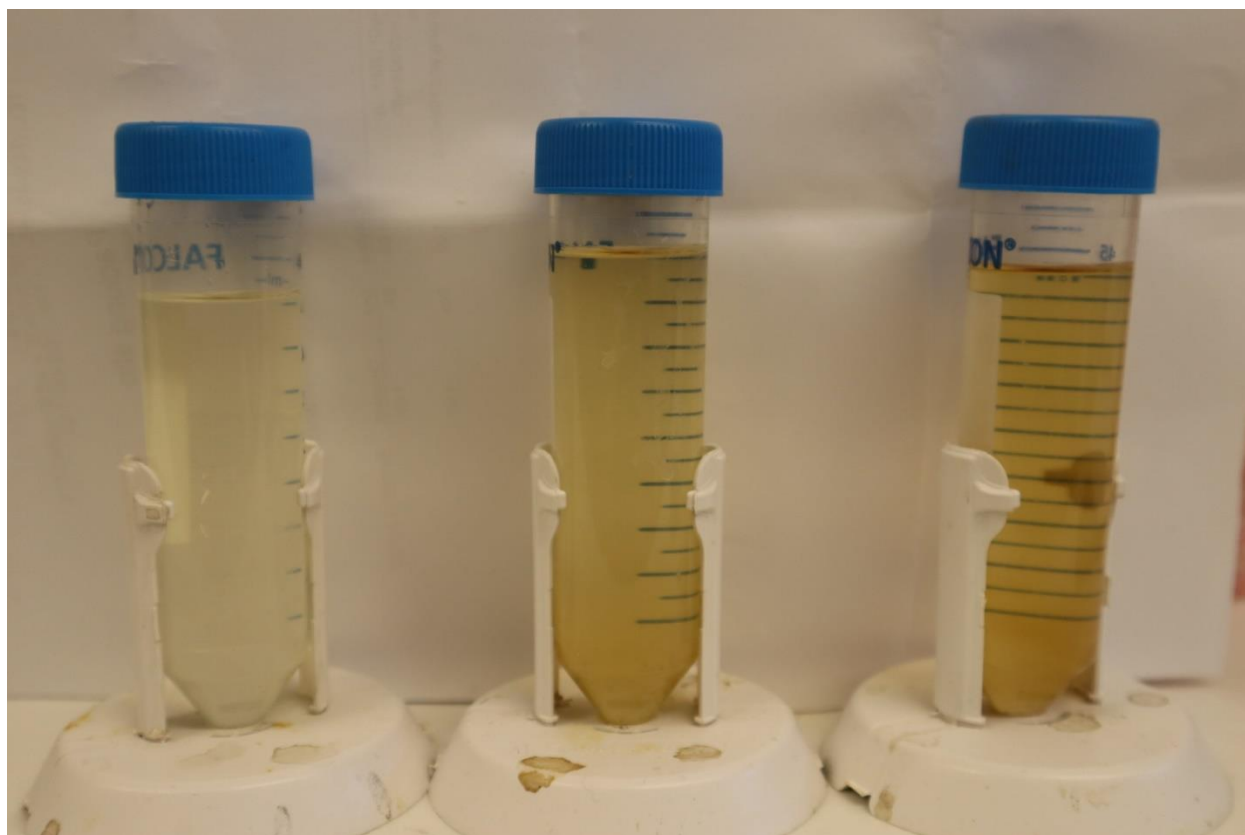


Figure 3.12. 6M KOH after various amounts of time performing cyclic voltammetry with copper tape substrate which exhibits a large degree of corrosion.

In order to circumvent this problem, nickel foam was used as the active current collector for the system. The primary benefit of nickel foam is that it is electrochemically inert at the voltage window in question, but the secondary benefits are that the nickel foam is a porous material which may increase the surface area of the electrode and additionally is lighter and so in battery or supercapacitor applications may serve to lower the overall package weight.

### 3.4 Choice of Electrolyte

The choice of electrolyte can also have a sizeable effect on the performance of the supercapacitor or battery electrode that is being studied. Many different electrolytes have been proposed in literature as electrolytes for supercapacitors, but most electrolytes commonly fall into the categories of aqueous and solid/organic. The benefits of the aqueous electrodes are that they are incredibly easy to produce, most are some forms of salt, and are safer (meaning less likely to

catch fire) than standard solid electrolytes. However, the energy that can be stored inside of an aqueous electrolyte is much lower than that of a solid or organic electrolyte due to the higher operating voltages that these can achieve because of the hydrogen evolution reaction of water that occurs around 1.2 Volts potential. Noting that, looking at

Table 2.2, the most common aqueous electrolytes are potassium hydroxide and sulfuric acid which is primarily due to their incredibly high electrical conductivity. Another benefit of the aqueous electrolytes are the relatively small ion diameter and electrical conductivity exhibited by these materials [79]. Below, in Figure 3.13, are graphs of the performance of a standard electrode in several different electrolytes at the same voltage window to compare performance.

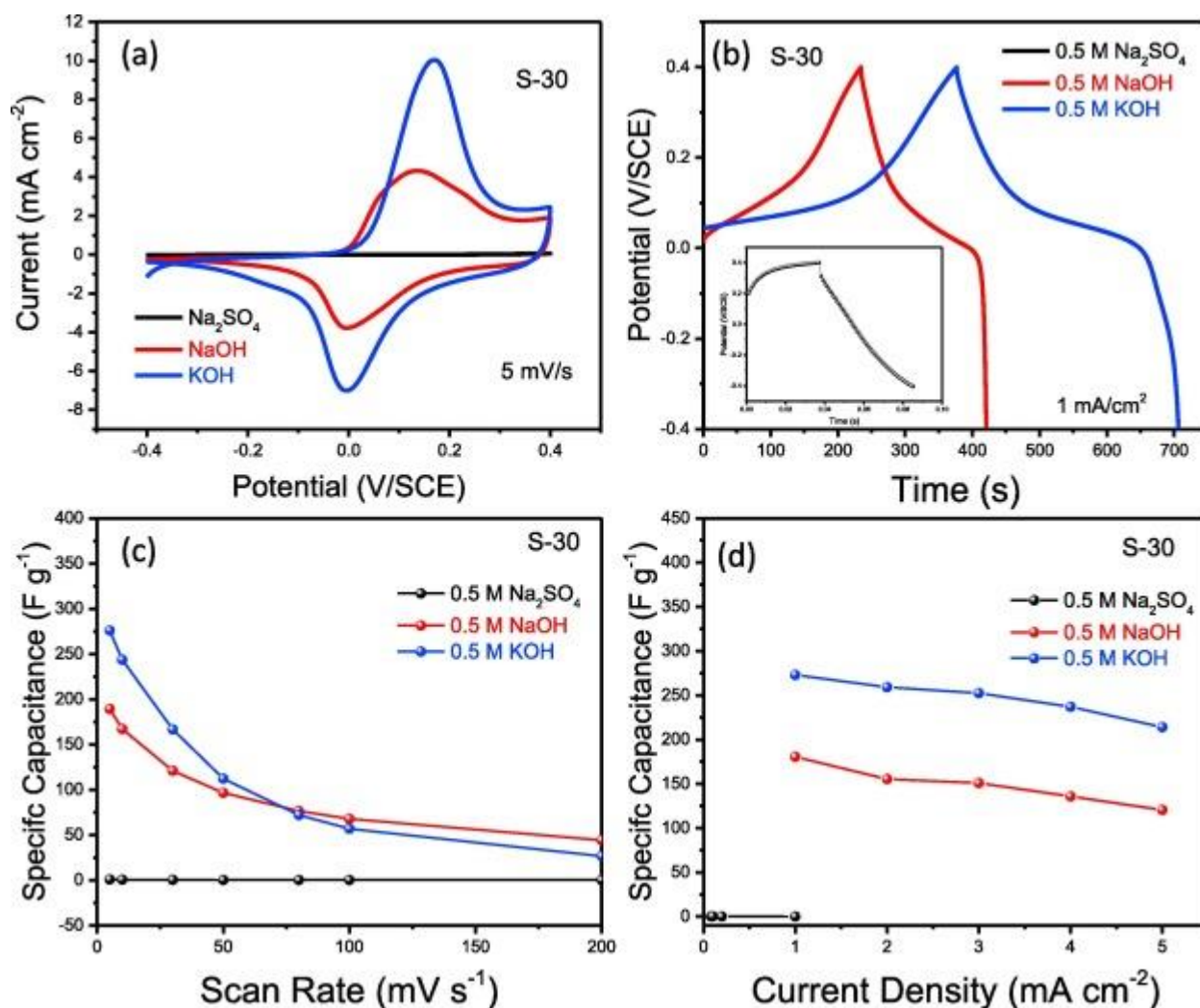


Figure 3.13. Figure showing the effect of electrolyte on the performance of the electrolyte on a Co(OH)<sub>2</sub> electrode. Used with permission of Elsevier under the <http://creativecommons.org/licenses/by-nc-nd/4.0/> from [80]

## 4. RESULTS AND DISCUSSION

### 4.1 SEM Imaging

SEM imaging was used to gain a clearer understanding of the surface topology and the structure of the composite was formed during the experiments. To perform these experiments, three different samples were taken throughout the sample creation process. The first sample was taken after the carbon nanotubes were redispersed in DMF after the centrifugation to remove the ethanol and water. The second sample was taken after the 48 hours of ZIF-8 synthesis in the oven. The final sample was taken after the addition of MoS<sub>2</sub> and the 24 hours that it was allowed to synthesize in the oven. This sample set gives clear images of how the sample changes with the addition of the 3 important energy materials. These images can be found in the following three figures: Figure 4.1, Figure 4.2, and Figure 4.3. Each figure is shown at two different magnifications with the higher magnification being shown second.

The first figure is of the carbon nanotubes sample. These images of the three show the smallest diameter, which is to be expected due to nanotubes not having been coated with ZIF-8 yet. Additionally, it can be observed that the average pore size appears to be slightly larger than the other two, likely because the additional of ZIF-8 creates a slightly thicker material that stacks in a different way that builds a nanotube forest in such a way that fills in some of the gaps.

The second sample, shown as Figure 4.2, shows the ZIF-8 framework deposited on the carbon nanotubes. This sample shows an appreciable increase in the diameter of the structure cause by the addition of ZIF-8 upon the carbon nanotube forest. The other striking feature of these images is the uniformity with which the ZIF is distributed over the carbon nanotubes. This relatively uniform distribution shows that the material is being equally distributed and bodes well for the properties of the material for energy storage.

The final image, Figure 4.3, demonstrates the deposition of MoS<sub>2</sub> onto the structure. As can be seen, the flakes of MoS<sub>2</sub> can be seen to be attached to the structure which demonstrates the ability of the MoS<sub>2</sub> to sulfur bond with the ZIF-8 structure shown in the previous figure. It additionally shows no increase in impurities between the two steps. The two main drawbacks from the structure that can be taken from the images have to do with the size and distribution of the MoS<sub>2</sub> flakes. The flakes are relatively large in their number of layers and have a relatively

infrequent and sporadic distribution. This structure showed a very large capacitance, energy, and power, but this may be able to further be improved by adding additional sulfur vacancies to the  $\text{MoS}_2$  to induce additional bonding to the ZIF-8 structure. This could potentially fix both problems as the  $\text{MoS}_2$  would be less likely to restack with itself and become more likely to sulfur bond to the material. Additionally, a way of uniformly bonding the  $\text{MoS}_2$  to the ZIF-8 may result in a higher capacitive performance but may also come with the tradeoff of being much more difficult to create and thus increase the cost of producing the material.

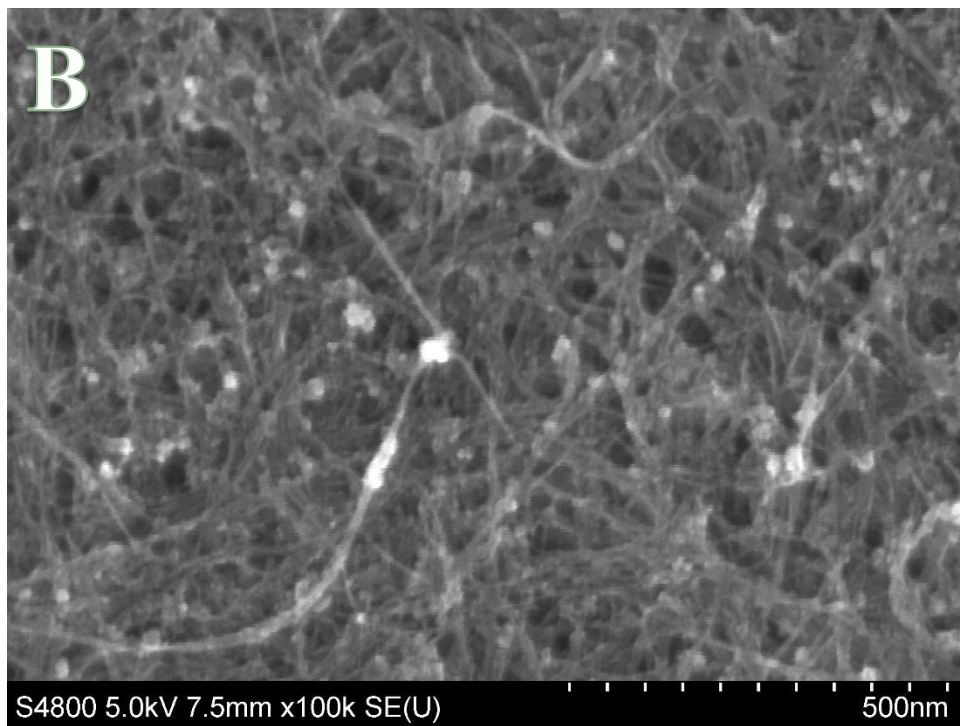
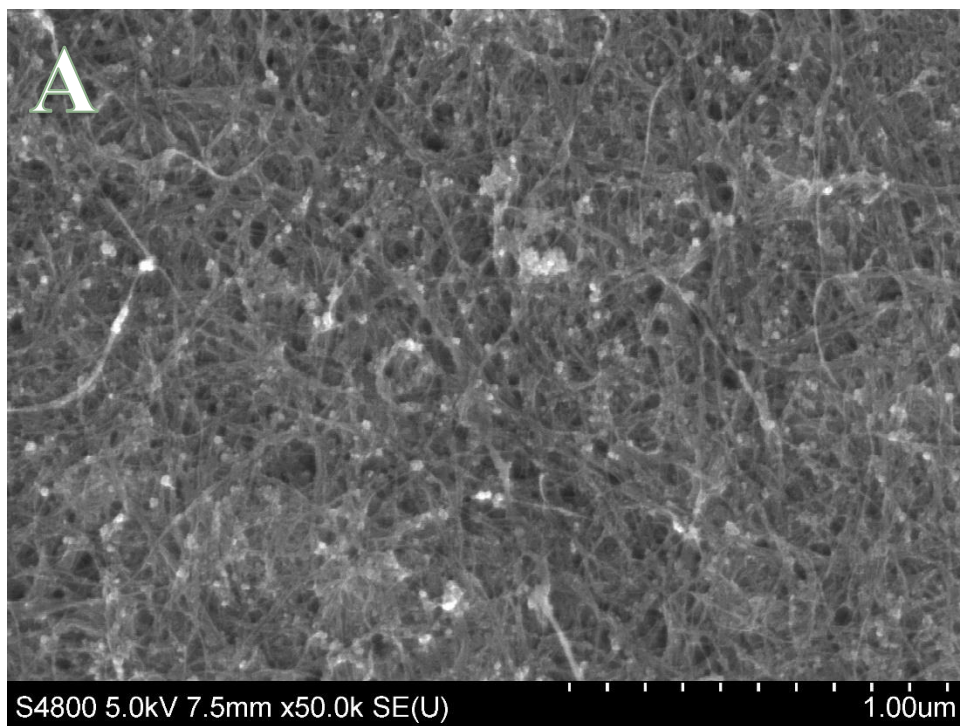


Figure 4.1. SEM images of the sample with only single walled carbon nanotubes at various magnifications of A (50x) and B (100x)

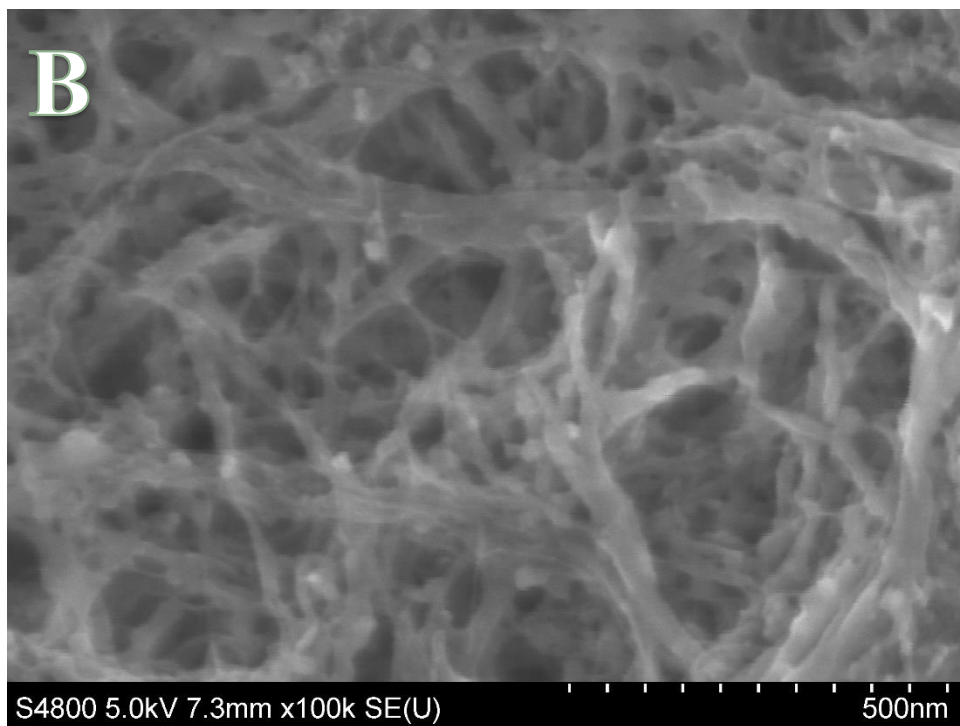
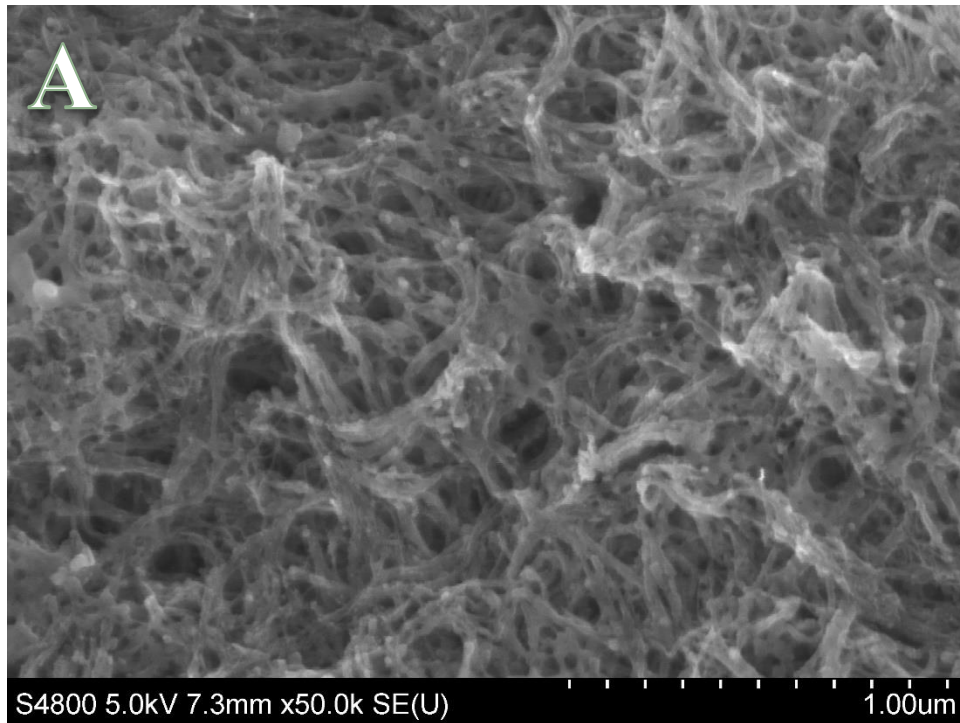


Figure 4.2. SEM images of the sample ZIF-8 bonded to carbon nanotubes at various magnifications of A (50x) and B (100x)

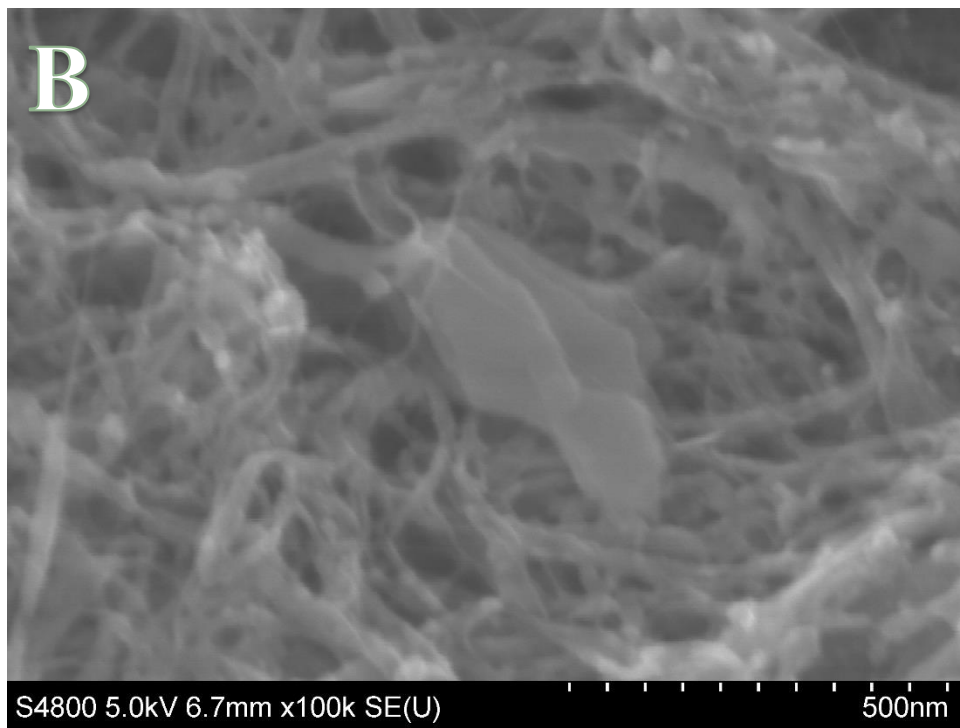
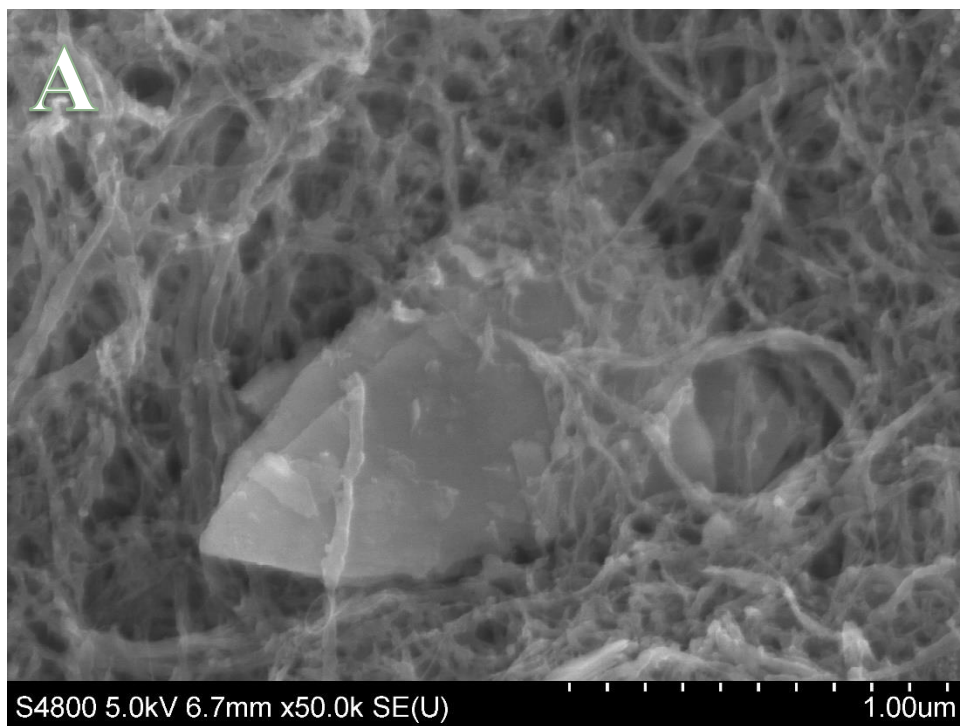


Figure 4.3. SEM images of the complete framework of CNT-ZIF-8-MoS<sub>2</sub> at various magnifications of A (50x) and B (100x)

## 4.2 Theoretical Capacitance Calculations

Based on the information that was found in the previous section and the information in the background section, a theoretical capacitance value can be attained for the material that was created with several large assumptions made. This analysis uses equation 2.3 from the Literature Review section of the report which says that the capacitance is equal to the product of the permittivity constants of free space, the permittivity of the electrostatic double layer, and the area of the electrode divided by the Debye length of the electric double layer [81].

To do these calculations the first thing to be determined is the specific area of the electrode. The area is difficult to determine based on the effect of the three different nanomaterials being used. The mass of the dopamine coated carbon nanotubes is very small (around 1/9<sup>th</sup>) the mass of the carbon nanotubes and dopamine. Because of this, if we assume that the surface of the dopamine coated carbon nanotubes is completely covered with ZIF-8. With this assumption the specific surface area is 0.9 times the surface area of ZIF-8 which is found in literature to be 1630 m<sup>2</sup>/g resulting in a total structural area of CNT-ZIF-8 of 1467 m<sup>2</sup>/g [70]. Finally, the surface area of the MoS<sub>2</sub> flakes that bond to the ZIF-8 must be determined. To do this we assume that all the layers of the MoS<sub>2</sub> are monolayers and that the monolayers cover approximately 15 percent of both the MoS<sub>2</sub> and the ZIF-8 surface area due to the sulfide bonding. The area for an average sized flake of MoS<sub>2</sub> from the SEM images can be found as approximately 304 m<sup>2</sup>/g from the density and thickness of the MoS<sub>2</sub> [82]. This results in a total structural area of around 1500 m<sup>2</sup>/g. The values of the permittivity of the 6M KOH that was used in the experiment is around 50 and the Debye length of the ZIF-MoS<sub>2</sub> material can be approximated as around 0.5[81]. This results in a theoretical capacitance of around 1330 F/g, the values found experimentally will always be significantly lower than the experimental values due to the coagulation effects of different nanomaterials as they are synthesized together in macroscopic applications.

### 4.3 Electrochemical Measurements

#### 4.3.1 Highest Performing Sample Measurements

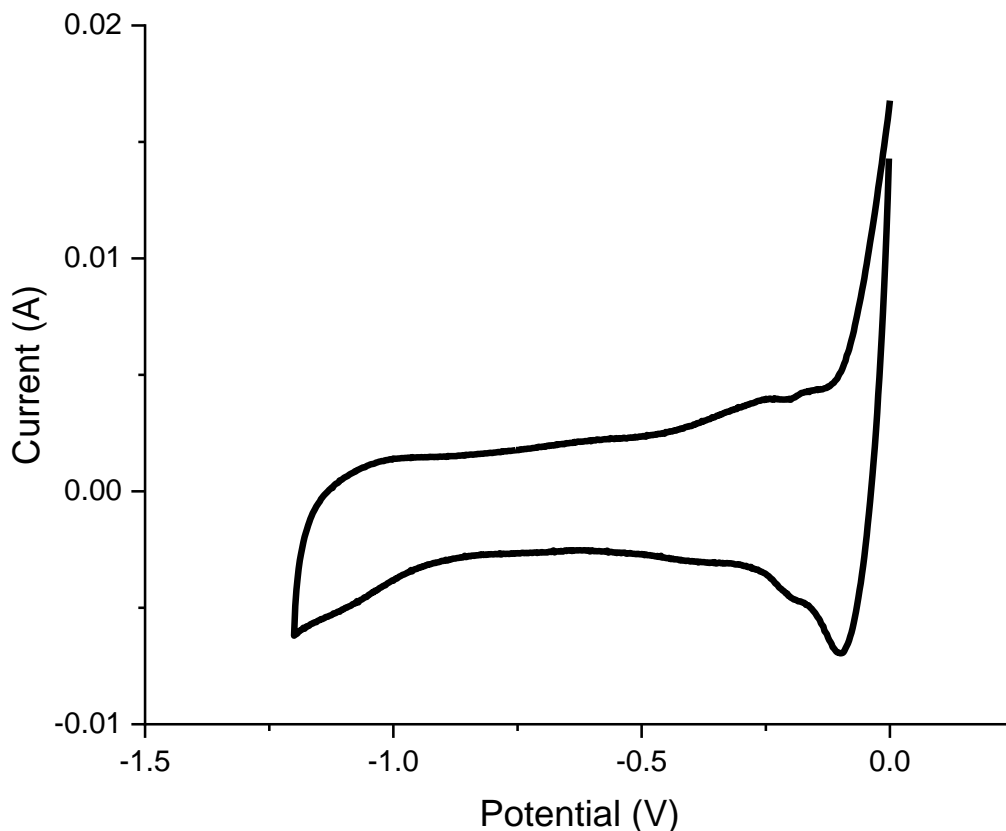


Figure 4.4. Cyclic Voltammetry graph showing the performance of the electrode at a scan rate of 20mv/s with a voltage window of 0 to -1.2V

Figure 4.4 shows the cyclic voltammetry curve of the highest performing sample that was tested as a part of this experiment. The sample was created according to the specifications of the procedure outlined in the experimental section. The mass of carbon nanotubes used to make the sample were 5mg single walled carbon nanotubes dispersed in approximately 20 ml of ethanol. The mass values for the ZIF-8 materials and MoS<sub>2</sub> are 15mg 3-thiol and 30 mg zinc chloride, and 10 mg MoS<sub>2</sub>. The entire solution was not used to create each individual sample, only around 3 ml of the sample was used to make each individual sample which also kept the mass of each sample

at 1 mg. This was confirmed by weighing the samples before and after the electrode material was deposited and the individual mass of the electrode film was determined to be around 1mg.

To produce the graph shown above, a voltage window of 0 V to -1.2 V and a scan rate of 20 mV/s were used. The scan rate was selected to be 20mV/s because this creates the highest energy density and capacitance while also providing a practical applicability and an appropriately large power density. Lower scan rates could potentially be used and would more than likely result in higher capacitance and energy values, but they often produce a much lower power density which is the advantage of supercapacitors compared to battery electrodes and so that advantage should be kept by maintaining a reasonable scan rate.

Using equations 2.4-2.11 from the background section, the specific capacitance of this sample can be calculated to be 262.15 F/g with corresponding specific energy and specific power values of 52.4 Whr/kg and 1572 W/kg respectively. The sample has a diameter of around 1cm and so the areal capacitance would be around 262.15 F/cm<sup>2</sup>. This project compares favorably to the different capacitor technologies that were listed out in Figure 2.2. The values of specific capacitance of 262.15 F/g compares very favorably to all of the nano-carbon only technologies for energy storage and additionally compares very well to all the ZIF based capacitors as well, with a specific capacitance value that is the highest or close to the highest value in the papers observed, many of which have much lower scan rates which would predict a much higher energy but would not reflect the practical use cases of a supercapacitor. The supercapacitors listed in the section that have transition metal dichalcogenides have very high stratification in the observed results, with the values split between the 1000s and the low 100s in range with the supercapacitor proposed here. The reason for this stratification is in the performance of these materials. The materials that have high very high specific capacitance values often exhibit a much more pseudocapacitive performance that results in a much quicker degradation of performance and compares more to a battery in terms of performance lifespan than an electric double layer capacitor. When observing the graphs that have cyclic voltammetry of charge-discharge graphs more in line with electrostatic double layer capacitors, the values for these electrostatic double layer capacitors is similar to the values found in this paper.

The values that have been calculated for the specific and areal capacitance and energy indicate that these technologies might be very applicable in the electric vehicle or electric train design where weight is not necessarily as important as volume for energy storage in order to give

an optimal area for storage for both passengers and objects. The primary use for the supercapacitor in this application would be to largely smooth out the large power fluctuations that are required during driving or between train stops, as these power fluctuations can have adverse reactions on the battery systems of trains including thermal fluctuations and increased irreversible effects due to rapidly cycling between charging and discharging [83] [84]. Supercapacitors, however, do not have this issue as they electrostatic double layer capacitors have a nearly irreversible charge transfer and storage process. And additional consideration of using supercapacitors would be the cost associated with using them in conjunction with batteries. Economic analysis of the supercapacitor battery hybrid energy storage systems predicts that supercapacitors will likely have to decrease in price to between 0.5 and 1.0 cents/F could be competitive with lithium ion batteries [85]. In addition to carbon being less expensive than lithium and the different metals that it is paired with in modern next generation lithium metal batteries, a significant cost advantage of supercapacitors could be found by substituting different steps in the manufacturing process. The process proposed would reduce the cost of manufacturing significantly by replacing the high temperature calcification step that usually accompanies the manufacturing of these materials with a much less intense vacuum filtration process.

Similar to the discussion above, this technology could also be applicable in electric aircraft, where there are large spikes in power required for takeoff and landing that would place a large amount of stress on the battery being used to power the system. Similar to how supercapacitors have been used above to account for high power fluctuations, this film could be used for this application as well due to meet those demands and lower the stress on the battery. This specific electrode made during this project can help in this regard as well have the advantage of a low cost per farad, however, for flight, weight becomes significantly more important and so more likely, supercapacitors with a lower specific capacitance could be used to fill this application.

Figure 4.5. Durability of the electrode over 30000 cycles. This shows relatively little degradation in performance over a larger number of cycles. below shows the behavior of the capacitor over 30000 cycles to test the durability of the material. It can be observed from this figure that the behavior of the capacitor is in line with that of an electrostatic double layer capacitor and not a pseudocapacitor. This can be determined both by the shape of the cyclic voltammetry curve and the from the behavior of the material as the cycle number increases. The shape of the cyclic voltammetry graph is expected to be box like, and this behavior is shown in the graph below with

the exception that the box is slightly slanted down. This is not necessarily an atypical behavior for supercapacitors though and is seen to varying degrees in other supercapacitor graphs. Additionally, the behavior of the supercapacitor changes very little as the number of cycles increases drastically, there is a small shift in the graph and specifically the angle that it makes with the horizontal, but the performance in terms of specific capacitance is largely unaffected. To perform this test, the number of cycles on the machine was increased significantly and the sample was observed, and all other conditions were kept constant.

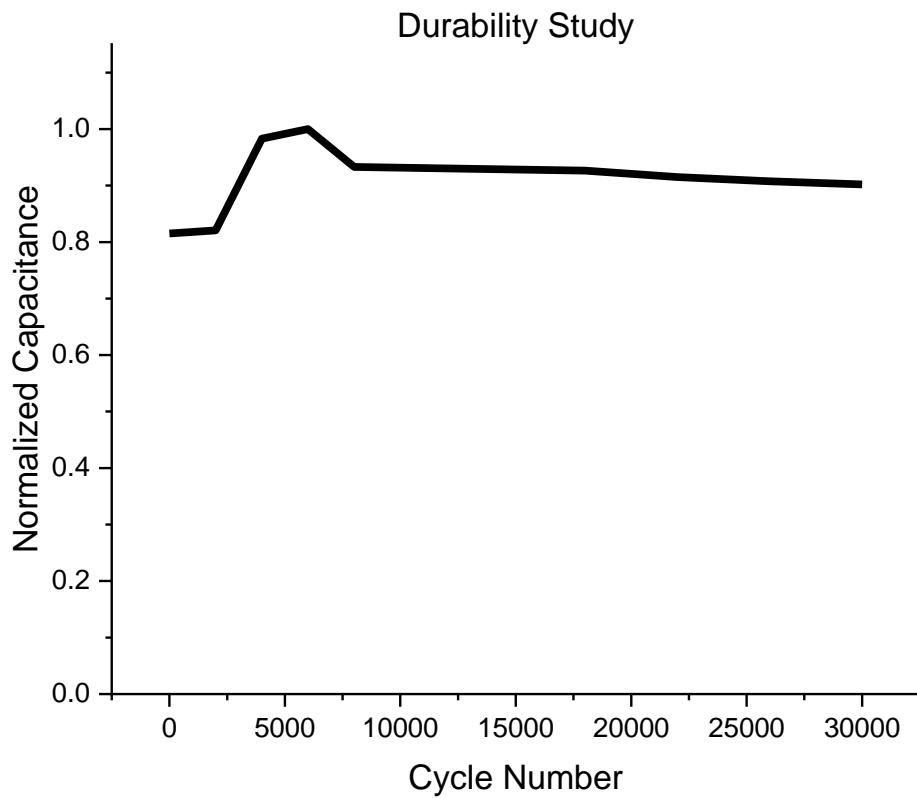


Figure 4.5. Durability of the electrode over 30000 cycles. This shows relatively little degradation in performance over a larger number of cycles. Normalized against the value of the capacitance at 30000 cycles.

### 4.3.2 Variable Scan Rates Results

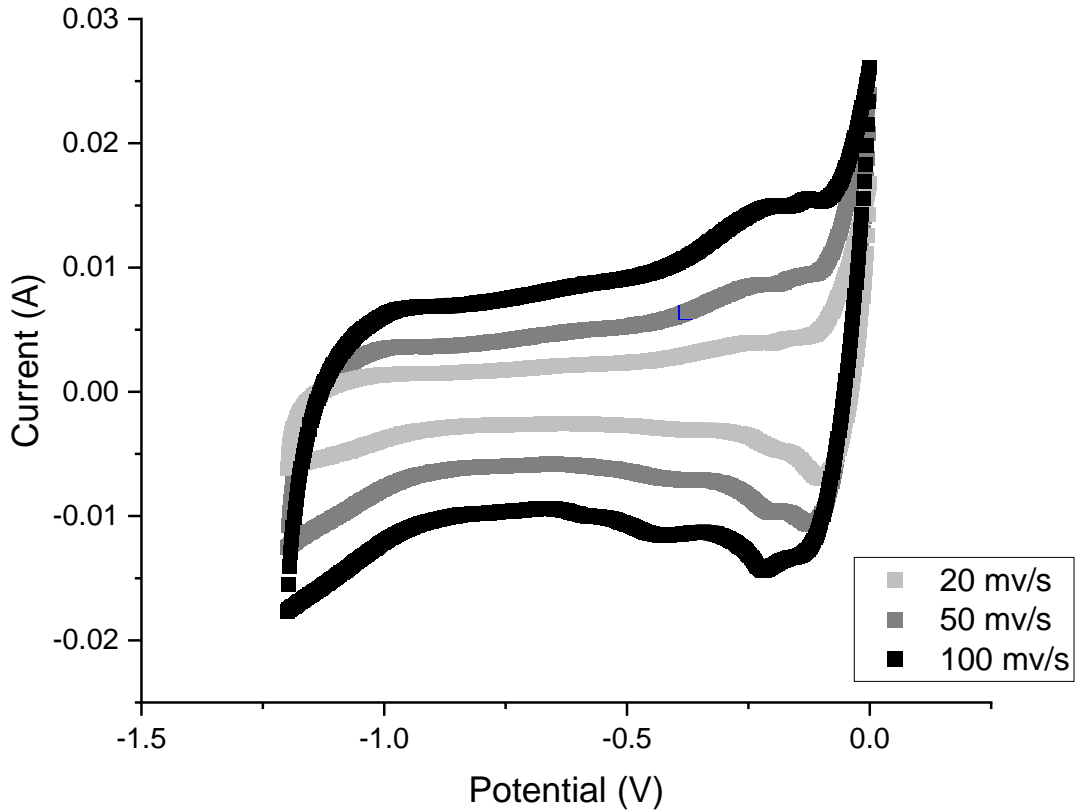


Figure 4.6. Cyclic Voltammetry graph of the electrode at various scan rates to show the change in performance that can be achieved by altering the scan rate.

The above figure, Figure 4.6, shows the performance of the supercapacitor electrode at several different scan rates. This data is typical for a supercapacitor electrode and is the type of data that should be expected for a supercapacitor electrode as increasing the scan rate has been found to favorably impact the capacitance of the electrode and specific and areal energy of the supercapacitor electrode at the expense of the specific and areal power. However, this increase cannot always be accounted for in the practical limits of use cases for supercapacitors because they are largely designed to be implemented to provide large power which decreases sharply with decreases in the scan rate of the sample as can be seen in the Ragone chart in Figure 4.7. This data is very similar to the data that other supercapacitor electrodes have shown at various scan rates and adds additional evidence to the performance of this electrode being capacitive in nature.

Another way to represent the variable scan rate data is to plot the results on a Ragone chart which has been seen and used several times throughout the paper to compare the energy and power values of several types of energy storage devices. There is an additional plot of the Ragone chart showing the specific energy and power values of this supercapacitor electrode superimposed on a Ragone plot from earlier in the presentation comparing the performance of other energy storage devices and the other supercapacitor electrodes shown below in Figure 4.8. What can be seen from observing this chart is that the plotted curve for this graph performs significantly better than commercial supercapacitors available for both energy and power and compares favorably as well to many of the different supercapacitors that have been researched as well. The performance is in the region of the graph with lithium capacitors, which are a type of hybrid pseudocapacitor which uses lithium (a common battery electrode) and has irreversible redox effects.

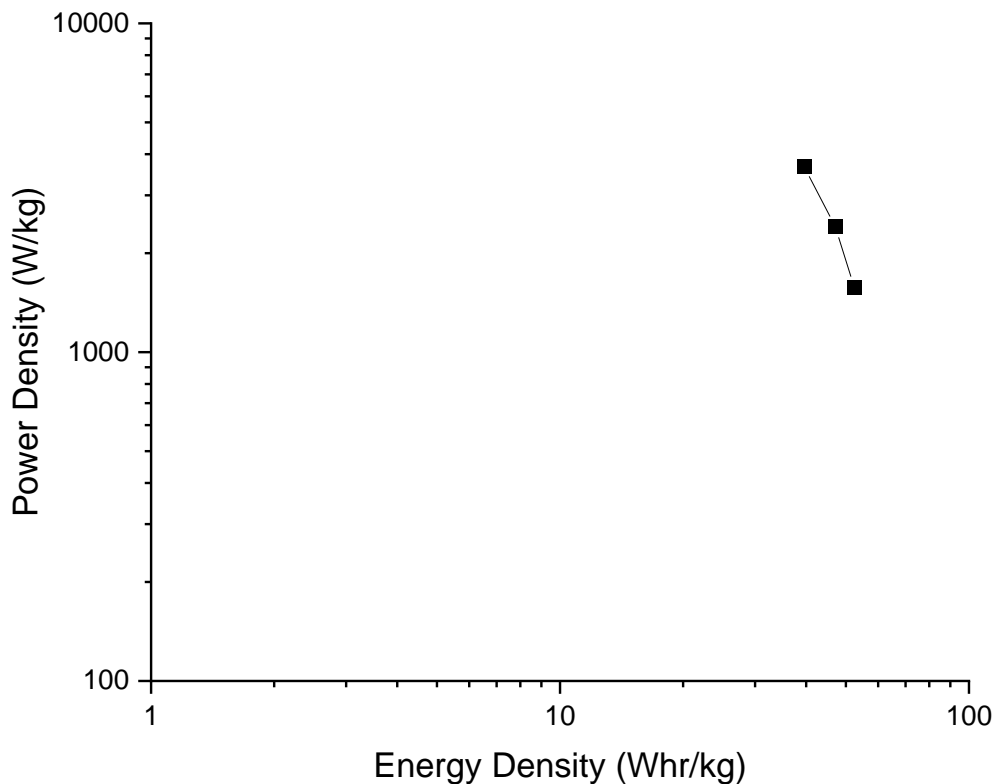


Figure 4.7. Ragone chart with performance of the supercapacitor at various scan rates to show how energy and power change with scan rate from 100mV/s as the top point to 20mV/s as the point with the lowest power density.

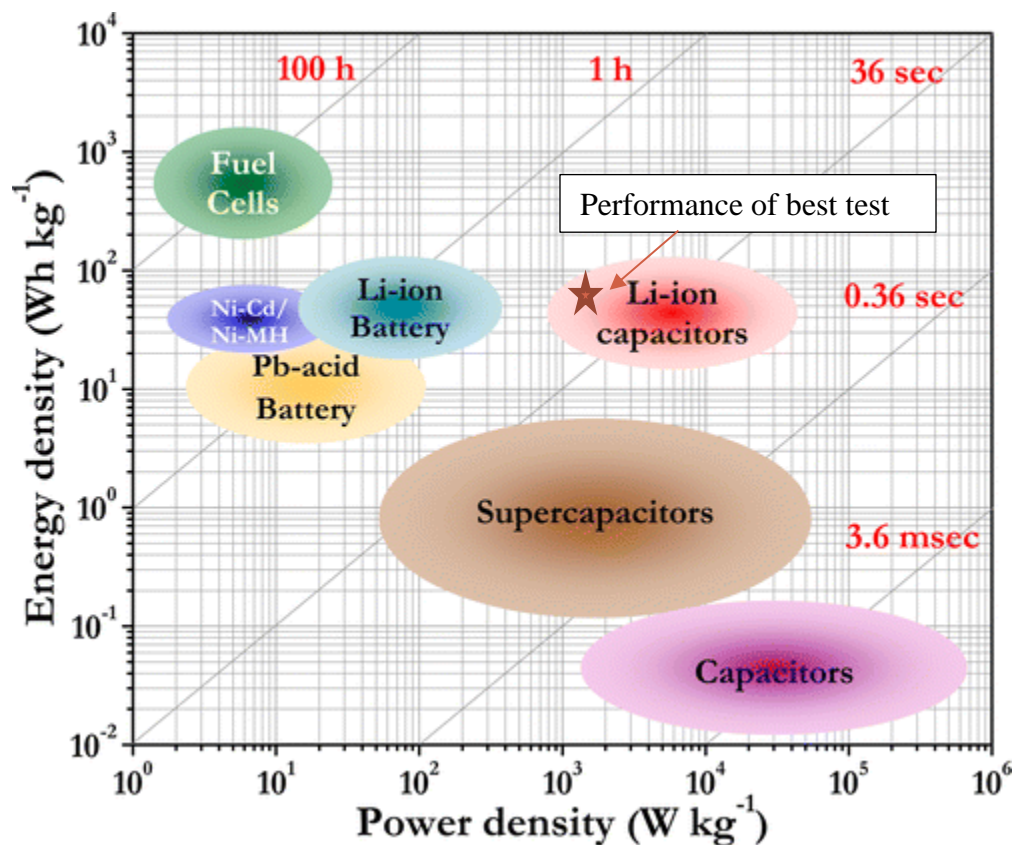


Figure 4.8. Ragone chart from the introduction with the point for the sample taken at 20mV/s graphed as well to show performance relative to other energy storage techniques. This figure is taken from [28] image used with the rights and permissions from ACS publishing.

### 4.3.3 Analysis of ratio of MoS<sub>2</sub>: ZIF-8 ratio

In addition to testing the energy and power of the supercapacitor electrode, tests were conducted to determine how the ratio of MoS<sub>2</sub> to ZIF-8 would affect the specific and areal capacitance of the sample. The results are found on Table 4.1 below, the normalized capacitance value is the capacitance of each sample divided by the capacitance of the highest performing sample, in this case, the sample with a mass ratio of 0.4:

Table 4.1. Table comparing values of the mass ratio of MoS<sub>2</sub> to ZIF-8 to capacitance.

MoS <sub>2</sub> :3-thiol (ZIF-8)	Normalized Capacitance
0.133	0.36
0.200	0.4
0.267	0.64
0.400	1
0.467	0.86
0.600	0.78
0.667	0.39

To conduct these tests, the mass ratio of carbon nanotubes to ZIF-8 was held constant while the mass ratio of ZIF-8 to MoS<sub>2</sub> was varied in order to determine the optimal amount of MoS<sub>2</sub> that could bond to the ZIF-8 coated carbon nanotubes as there would only be a set number of sulfur vacancies inherently present in the MoS<sub>2</sub>. In other words, as long as the masses of carbon nanotubes and ZIF-8 are held constant, the structure should theoretically look very similar and have the relative same number of bonding sites as long as the preparation steps are the same. In addition to keeping the two masses above held constant, one bulk sample of ZIF-8 coated carbon nanotubes was prepared and then divided into 7 different samples to ensure uniformity to the best possible degree. To quantify the mass ratio of ZIF-8 because it is a synthesis of two different chemicals and cannot be directly measured, the mass of 3-thiol-1,2,4 triazole was used as a substitute.

The result of this ratio study is that the capacitance of the sample electrodes seems to peak at mass ratio of around 0.4 mg MoS<sub>2</sub> to ZIF-8. The behavior of the mass ratio is illustrated graphically in Figure 4.9 showing very clearly the peak performance at the ratio of 0.4. The capacitance of the sample seems to increase until a certain point and then continue to decrease afterwards before reaching a lower plateau value. The increasing behavior can be explained by considering the saturation of MoS<sub>2</sub> bonding to the ZIF-8 framework. Until a certain point, there will be additional bonding sites of the ZIF-8 framework which could be used to bond MoS<sub>2</sub>, however, once the bonding sites of the ZIF-8 have been fully saturated with MoS<sub>2</sub>, the additional MoS<sub>2</sub> will reform its Van der Waals with other MoS<sub>2</sub> increasing the thickness of the MoS<sub>2</sub> which

will subsequently reduce the surface area to volume ratio and the unique values of few-layered MoS<sub>2</sub> including the already poor conductivity.

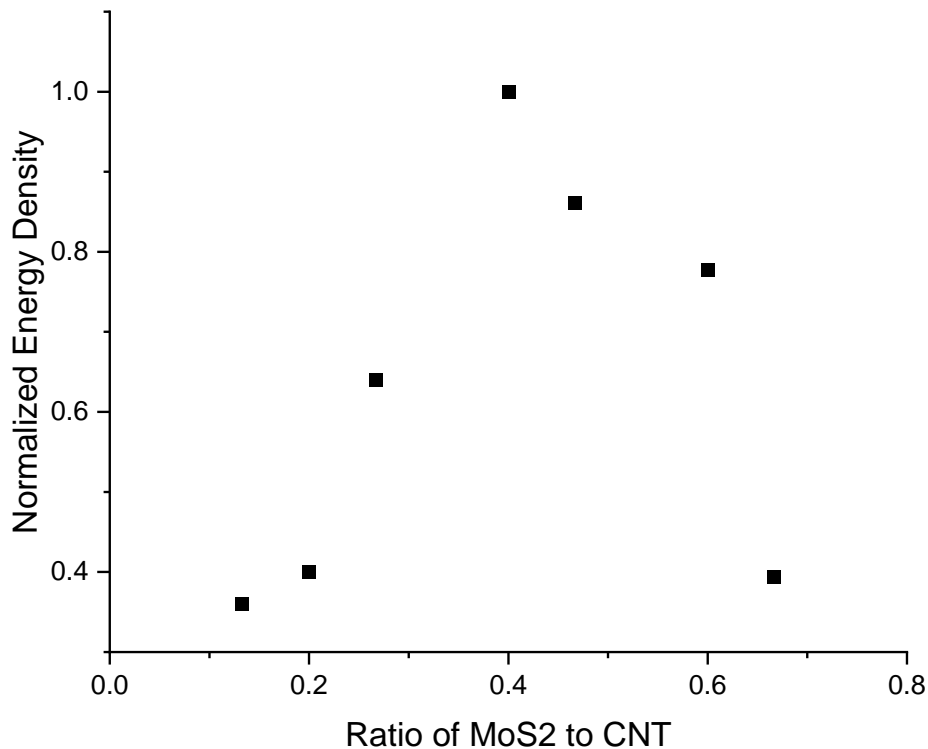


Figure 4.9. Figure of the plotted data from Table 4.1. showing the graphical relationship between performance and the ratio of MoS<sub>2</sub> to ZIF-8.

#### 4.3.4 Analysis of ratio of ZIF-8: Carbon Nanotubes

In addition to testing the ratio of ZIF-8 to MoS<sub>2</sub> the ratio of carbon nanotubes to ZIF-8 was also determined to find how the performance of the supercapacitor varies with additional levels of the ZIF-8. Table 4.2 below summarizes the results of the study to determine the optimal ratio of materials with the ratio of the masses of ZIF-8 (mass 3-thiol) to carbon nanotubes being reported in the left column and the capacitance, normalized to the against the value of the highest performing sample (in this case the ratio of 3:1).

Table 4.2 Table comparing values of the mass ratio of carbon nanotubes to ZIF-8 to capacitance.

3-thiol (ZIF-8): Carbon Nanotubes	Normalized Capacitance
1.0	0.6
2.0	0.76
3.0	1.00
4.0	1.02
5.0	0.97

The test is important because it can inform on the structure and the ratio that achieves the best performing structure of the material using our preparation steps. The mass of carbon nanotubes is fixed by choice, and therefore there will be a specific mass of ZIF-8 materials that produces enough ZIF-8 to fully coat the carbon nanotubes with ZIF-8. This full coating will also allow the greatest number of optimal sites of bonding for the MoS<sub>2</sub> flakes. In terms of the behavior of the material, it appears from the data that the performance of the capacitor increases up until a mass ratio of about 3 mg ZIF-8 per mg carbon nanotubes. The mass of ZIF-8 is expressed as it was in the last section as the mass of 3-thiol. After the ratio reaches the peak value around a ratio of 3 mg ZIF-8 per mg of carbon nanotubes the value plateaus at a normalized energy density value of approximately one. This occurs because more than likely, once the carbon nanotubes have been completely coated, the capacitance gains from adding additional ZIF-8 become much more marginal and become offset by the increase in mass of the electrode. This information is also shown below which graphically represents the values of this table and which can be clearly shows the plateau of the performance with respect to mass.

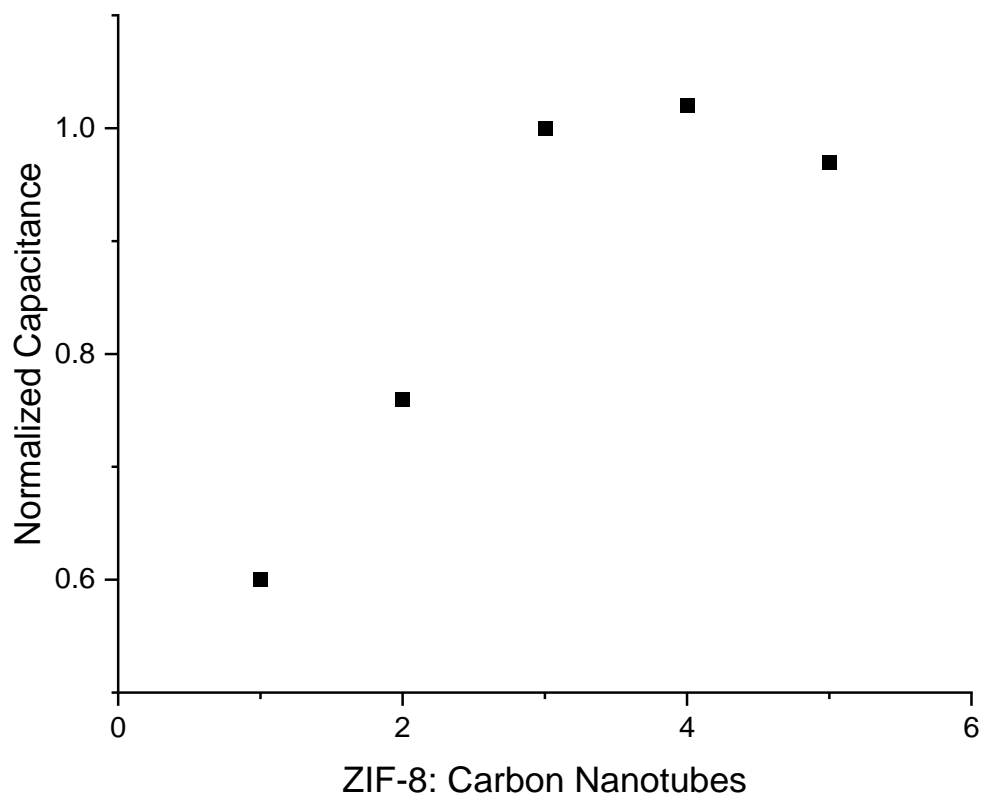


Figure 4.10. Figure of the plotted data from Table 4.2. showing the graphical relationship between performance and the ratio of CNT to ZIF-8.

### 4.3.5 Comparison of Materials at Every Phase of Production

Table 4.3. Comparison of the performance of the sample at several different stages of production

Sample	Specific Energy (Whr/kg)	Specific Capacitance (F/g)
CNT	3.7	18.7
CNT-ZIF-8	21.2	105.9
CNT-MoS <sub>2</sub>	14.5	72.5
CNT-ZIF-8-MoS <sub>2</sub>	45.7	230.1

To prove the effectiveness of the addition of each material, the sample was tested at each phase in production to determine each material's relative effect on the performance of the electrode. The three stages that were tested were carbon nanotubes after dispersion in DMF, Carbon nanotubes after the ZIF-8 had been synthesized, and the normal electrode (with all three materials) in addition to a sample that was synthesized without the ZIF-8 coating. The specific energy of each of these materials is shown on middle column and the capacitance on the right. As should be expected, the sample with the highest specific energy is the sample with all three of the materials, followed by the sample that is only missing the molybdenum disulfide, followed by the sample only containing carbon nanotubes. The results of these experiments are summarized in Table 4.3 above and are represented graphically in Figure 4.11 along with a graph of the carbon nanotubes and molybdenum disulfide without the ZIF-8.

These values match (or are on the order same order of magnitude as) the values of several papers or other projects that have looked at these materials individually. For example, the highest values of capacitance seen for carbon nanotubes reaches around 15 F/g, but many of these values are taken using organic electrolytes which result in a higher capacitance value than the one that we determined and additionally have more optimized their process for the use of carbon nanotubes as that is the only material of interest [86]–[88]. Additionally, comparing the values to the reported values in the background section. The reported value for the CNT-ZIF section is within the range of values that are to be expected for the material, between 100 and 300 F/g. The increase in capacitance seen after the addition of each different material shows the potential utility of each

and how the materials combine to form a supercapacitor that has a much higher specific capacitance than any material individually.

The improvement in performance that is seen by combining all three of the nanomaterials makes the material competitive with many of the supercapacitors that are being reported in literature. The similarity of this supercapacitor electrode in performance to its peer supercapacitor electrodes is very encouraging as it signals that the preparation method used for this electrode which is much less labor and fiscally intense can be possible to create a less expensive, high performing supercapacitor electrode in the future which could compete more effectively with battery technologies and reach the 50 to 100 Cent/F price point that will make them specifically much more competitive in the electric vehicle space.

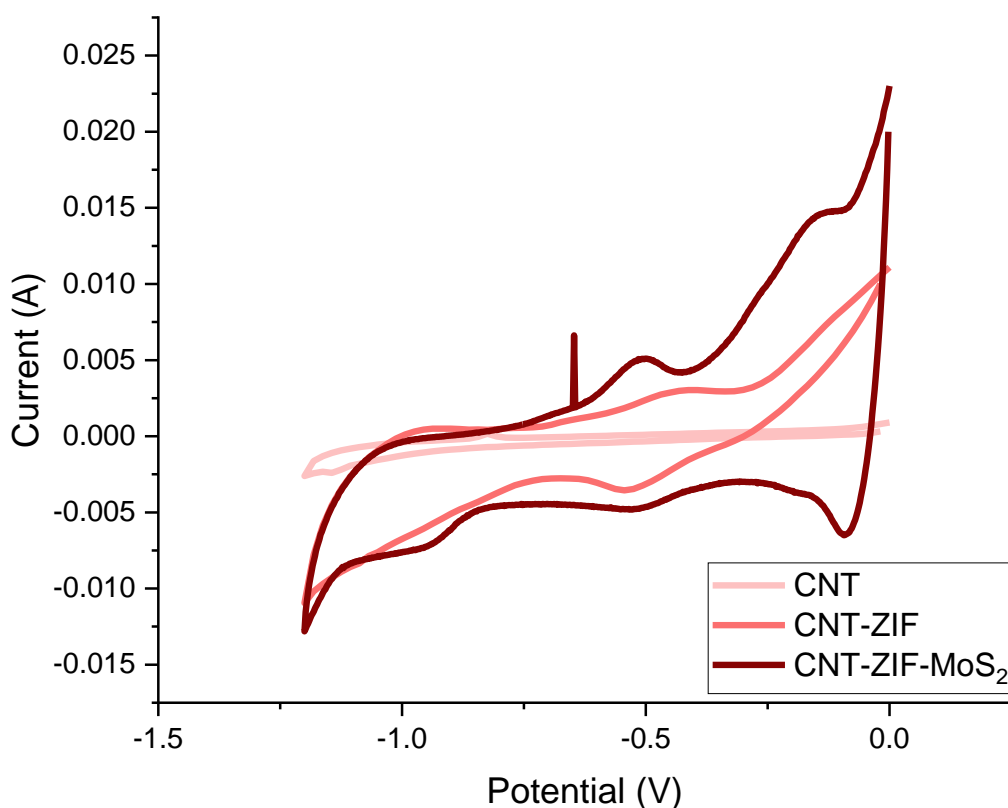


Figure 4.11. Cyclic voltammetry graph of 1 cycle for each material at various stages of production including CNT only, CNT-(ZIF-8), and CNT-(ZIF-8)- MoS<sub>2</sub>.

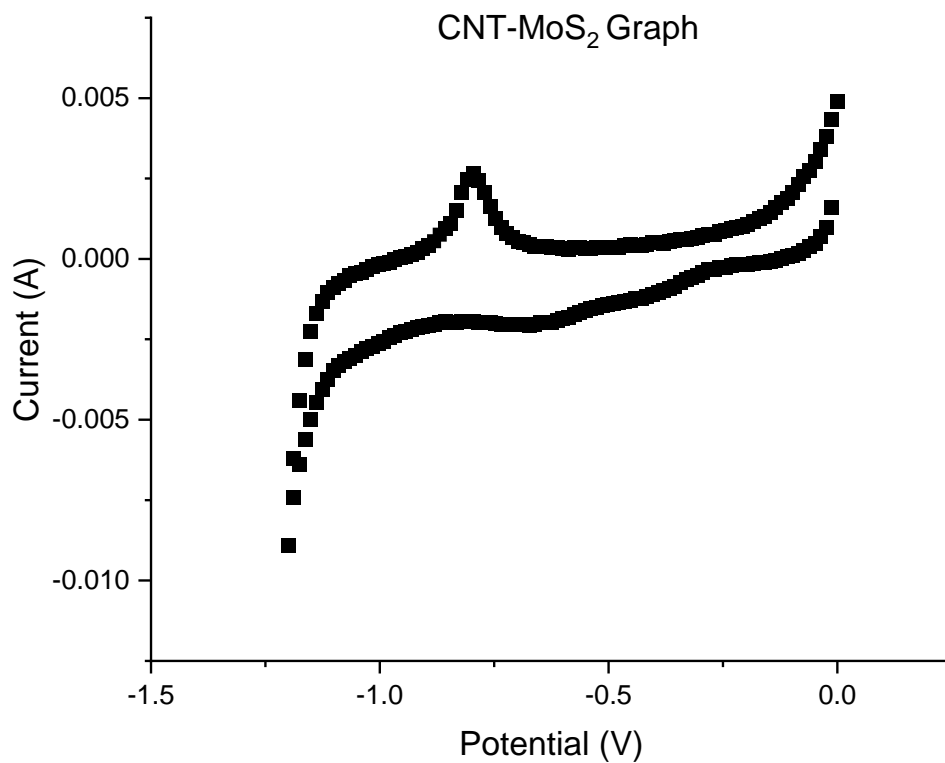


Figure 4.12. Graph of only carbon nanotubes and molybdenum disulfide without the ZIF-8 present, notice that the capacitance of this data is also lower than the value of the combined material.

## 5. CONCLUSION AND FUTURE WORK

### 5.1 Conclusions

Nanomaterials have for a long time been studied for their unique and promising properties at incredibly small dimensions. Several of these properties include a very high surface area to volume ratio and good charge storage capacity. These characteristics make these materials very well suited to serve as supercapacitor materials as both the pseudocapacitor and electrostatic double layer capacitor performance is improved with higher surface area and good conductive and charge storage material.

This project utilized three different nanomaterials that have unique properties that when combined project to form a very well performing supercapacitor. All these materials have very large surface area to volume ratios, but individually, carbon nanotubes have a high electrical conductivity, metal organic frameworks (ZIF-8) have a strong ion diffusivity, and transition metal dichalcogenides ( $\text{MoS}_2$ ) have good charge storage capability. Additionally, these materials were chosen for their ability to bond together via the sulfur bonding on the ZIF-8 to the sulfur vacancies present in the few layered  $\text{MoS}_2$ .

These electrodes were created using centrifugation and vacuum filtration process instead of a longer evaporation process and high temperature calcification resulting in a much faster and less expensive process. Additionally, this proposed framework was shown to confirm the theory that these materials can combine and form a high performing supercapacitor electrode as seen in the SEM images in the results section and the CV graphs which show a specific capacitance, energy and power of 262.15 F/g, 52.4 Whr/kg, and 1572 W/kg, respectively. The material also saw improvements in performance at each step of the process justifying the use of all three materials and not any subset of them. This electrode has practical limits to its performance due to the method of preparation, but even with these faster preparation steps was shown to have a specific capacitance value that rivals that of other researched materials present in the literature survey section.

## 5.2 Future Work Considerations

There are several different directions that this project could take moving forward based on the different novelties of the experiment: the preparation method, the materials, and the overall device prediction.

If the preparation method is to pursue, it would be interesting to do a comparison study between the method of preparation proposed in this study, and some other preparation methods seen in the literature. Additionally, this might be able to be expanded and it could be found that a higher performance is possible by carbonizing the ZIF-8 which has been shown to increase the performance in other supercapacitor electrodes but also requires hot temperatures and a reduced nitrogen (inert) environment.

Additionally, if the materials are to be considered, it would be interesting to see if other preparations of nanomaterials or different nanomaterials within the current families of carbon, metal organic framework, and transition metal dichalcogenide could be used and produce similar results. In terms of preparation, a more ordered sheet could potentially be created by growing carbon nanotubes naturally and then building the ZIF-8 and MoS<sub>2</sub> framework on top of the already present material. This would be a much more ordered structure and would theoretically have a much higher surface area which should increase capacitance. This concept could be extended to include other materials such as graphene or other transition metal dichalcogenides such as tungsten disulfide (WS<sub>2</sub>) which could theoretically be better performing.

Finally, this theoretical proposal of a single supercapacitor electrode could be extended into a created supercapacitor device test which would operate as a two-electrode system and could give a more realistic performance evaluation of the electrode in a real system modeling an actual device. This could also test several different setups between symmetrical and asymmetrical supercapacitor designs which could even potentially incorporate battery or pseudocapacitor electrodes to examine performance.

## REFERENCES

- [1] IEA (2020), *World Energy Outlook 2020*, IEA, Paris <https://www.iea.org/reports/world-energy-outlook-2020>.
- [2] T. M. Lenton *et al.*, “Climate tipping points — too risky to bet against,” *Nature*, vol. 575, no. 7784, Art. no. 7784, Nov. 2019, doi: 10.1038/d41586-019-03595-0.
- [3] S. Liu, L. Wei, and H. Wang, “Review on reliability of supercapacitors in energy storage applications,” *Applied Energy*, vol. 278, Nov. 2020, doi: 10.1016/j.apenergy.2020.115436.
- [4] G. Z. Chen, “Supercapacitor and supercapattery as emerging electrochemical energy stores,” *International Materials Reviews*, vol. 62, no. 4, pp. 173–202, May 2017, doi: 10.1080/09506608.2016.1240914.
- [5] A. Barhoum *et al.*, “A Broad Family of Carbon Nanomaterials: Classification, Properties, Synthesis, and Emerging Applications,” *Handbook of Nanofibers*, A. Barhoum, M. Bechelany, and A. Makhlouf, Eds. Cham: Springer International Publishing, 2019, pp. 1–40.
- [6] N. Saifuddin, A. Z. Raziah, and A. R. Junizah, “Carbon Nanotubes: A Review on Structure and Their Interaction with Proteins,” *Journal of Chemistry*, vol. 2013, p. 676815, Sep. 2012, doi: 10.1155/2013/676815..
- [7] A. H. Castro Neto, F. Guinea, N. M. R. Peres, K. S. Novoselov, and A. K. Geim, “The electronic properties of graphene,” *Reviews of Modern Physics*, vol. 81, no. 1, pp. 109–162, Jan. 2009, doi: 10.1103/RevModPhys.81.109.
- [8] S. Xie, W. Li, Z. Pan, B. Chang, and L. Sun, “Mechanical and physical properties on carbon nanotube,” *Journal of Physics and Chemistry of Solids*, vol. 61, no. 7, pp. 1153–1158, Jul. 2000, doi: 10.1016/S0022-3697(99)00376-5.
- [9] P.-C. Ma, N. A. Siddiqui, G. Marom, and J.-K. Kim, “Dispersion and functionalization of carbon nanotubes for polymer-based nanocomposites: A review,” *Composites Part A: Applied Science and Manufacturing*, vol. 41, no. 10, pp. 1345–1367, Oct. 2010, doi: 10.1016/j.compositesa.2010.07.003.
- [10] M.-F. Yu, B. S. Files, S. Arepalli, and R. S. Ruoff, “Tensile Loading of Ropes of Single Wall Carbon Nanotubes and their Mechanical Properties,” *Physics Review Letters*, vol. 84, no. 24, pp. 5552–5555, Jun. 2000, doi: 10.1103/PhysRevLett.84.5552.

- [11] X. Tang, L. Zhao, W. Sun, and Y. Wang, "Two-dimensional metal-organic framework materials for energy conversion and storage," *Journal of Power Sources*, vol. 477, Nov. 2020, doi: 10.1016/j.jpowsour.2020.228919.
- [12] S. Wu, L. Qin, K. Zhang, Z. Xin, and S. Zhao, "Ultrathin 2D metal-organic framework nanosheets prepared via sonication exfoliation of membranes from interfacial growth and exhibition of enhanced catalytic activity by their gold nanocomposites," *RSC Advances*, vol. 9, no. 17, pp. 9386–9391, 2019, doi: 10.1039/C9RA00662A.
- [13] W.-M. Liao *et al.*, "Tailoring exciton and excimer emission in an exfoliated ultrathin 2D metal-organic framework," *Nature Communications*, vol. 9, Art. no. 2401, Jun. 2018, doi: 10.1038/s41467-018-04833-1.
- [14] T.-J. Wang, X. Liu, Y. Li, F. Li, Z. Deng, and Y. Chen, "Ultrasonication-assisted and gram-scale synthesis of Co-LDH nanosheet aggregates for oxygen evolution reaction," *Nano Research*, vol. 13, pp. 79–85, Jan. 2020, doi: 10.1007/s12274-019-2575-5.
- [15] L. Jiao, J. Y. R. Seow, W. S. Skinner, Z. U. Wang, and H.-L. Jiang, "Metal-organic frameworks: Structures and functional applications," *Materials Today*, vol. 27, pp. 43–68, Jul. 2019, doi: 10.1016/j.mattod.2018.10.038.
- [16] Jia-ze Weng, Shi-yong Wang, Pei-xin Zhang, Chang-ping Li, Gang Wang, "A review of metal-organic framework-derived carbon electrode materials for capacitive deionization", *New Carbon Materials*, Volume 36, 2021, Pages 117-132, doi:10.1016/S1872-5805(21)60009-4.
- [17] D. J. Tranchemontagne, J. L. Mendoza-Cortés, M. O’Keeffe, and O. M. Yaghi, "Secondary building units, nets and bonding in the chemistry of metal-organic frameworks," *Chemical Society Reviews*, vol. 38, no. 5, pp. 1257–1283, Apr. 2009, doi: 10.1039/B817735J.
- [18] R. Ahmad, U. A. Khan, N. Iqbal, and T. Noor, "Zeolitic imidazolate framework (ZIF)-derived porous carbon materials for supercapacitors: an overview," *RSC Advances*, vol. 10, no. 71, pp. 43733–43750, Nov. 2020, doi: 10.1039/D0RA08560J.
- [19] S. Wu, Y. Du, and S. Sun, "Transition metal dichalcogenide based nanomaterials for rechargeable batteries," *Chemical Engineering Journal*, vol. 307, pp. 189–207, Jan. 2017, doi: 10.1016/j.cej.2016.08.044.

- [20] T. Stephenson, Z. Li, B. Olsen, and D. Mitlin, "Lithium ion battery applications of molybdenum disulfide (MoS<sub>2</sub>) nanocomposites," *Energy & Environmental Science*, vol. 7, pp. 209–231, 2014, doi: 10.1039/C3EE42591F.
- [21] H. Zhang, J. Ji, A. A. Gonzalez, and J. H. Choi, "Tailoring photoelectrochemical properties of semiconducting transition metal dichalcogenide nanolayers with porphyrin functionalization," *Journal of Material Chemistry*, vol. 5, no. 43, pp. 11233–11238, Nov. 2017, doi: 10.1039/C7TC02861J.
- [22] J. Ji, C. M. Delehey, D. N. Houpt, M. K. Heighway, T. Lee, and J. H. Choi, "Selective Chemical Modulation of Interlayer Excitons in Atomically Thin Heterostructures," *Nano Letters*, vol. 20, no. 4, pp. 2500–2506, Apr. 2020, doi: 10.1021/acs.nanolett.9b05254.
- [23] Chhowalla, M., Shin, H., Eda, G. *et al.*, "The chemistry of two-dimensional layered transition metal dichalcogenide nanosheets," *Nature Chemistry*, **5**, 263–275 doi: 10.1038/nchem.1589.
- [24] N. Choudhary *et al.*, "Two-dimensional transition metal dichalcogenide hybrid materials for energy applications," *Nano Today*, vol. 19, pp. 16–40, Apr. 2018, doi: 10.1016/j.nantod.2018.02.007.
- [25] D. Monga, S. Sharma, N. P. Shetti, S. Basu, K. R. Reddy, and T. M. Aminabhavi, "Advances in transition metal dichalcogenide-based two-dimensional nanomaterials," *Materials Today Chemistry*, vol. 19, Mar. 2021, doi: 10.1016/j.mtchem.2020.100399.
- [26] J. Ji and J. H. Choi, "Layer-Number-Dependent Electronic and Optoelectronic Properties of 2D WSe<sub>2</sub>-Organic Hybrid Heterojunction," *Advanced Materials Interfaces*, vol. 6, no. 17, 2019, doi: 10.1002/admi.201900637.
- [27] D. Voiry *et al.*, "Covalent functionalization of monolayered transition metal dichalcogenides by phase engineering," *Nature Chemistry*, vol. 7, pp. 45-49, Jan. 2015, doi: 10.1038/nchem.2108.
- [28] V. Aravindan, J. Gnanaraj, Y.-S. Lee, and S. Madhavi, "Insertion-Type Electrodes for Nonaqueous Li-Ion Capacitors," *Chemical Reviews*, vol. 114, no. 23, pp. 11619–11635, Dec. 2014, doi: 10.1021/cr5000915.
- [29] J. Zhang, L. Zhang, F. Sun, and Z. Wang, "An Overview on Thermal Safety Issues of Lithium-ion Batteries for Electric Vehicle Application," *IEEE Access*, vol. 6, pp. 23848–23863, 2018, doi: 10.1109/ACCESS.2018.2824838.

- [30] W. Cao, J. Zhang, and H. Li, “Batteries with high theoretical energy densities,” *Energy Storage Materials*, vol. 26, pp. 46–55, Apr. 2020, doi: 10.1016/j.ensm.2019.12.024.
- [31] R. Bansal, P. Menon, and R. C. Sharma, “Silicon–air batteries: progress, applications and challenges,” *SN Applied Sciences*, vol. 2, no. 6, May 2020, doi: 10.1007/s42452-020-2925-7.
- [32] A. K. Samantara and S. Ratha, “Historical Background and Present Status of the Supercapacitors,” in *Materials Development for Active/Passive Components of a Supercapacitor: Background, Present Status and Future Perspective*, A. K. Samantara and S. Ratha, Eds. Singapore: Springer, 2018, pp. 9–10.
- [33] A. G. Olabi, C. Onumaegbu, T. Wilberforce, M. Ramadan, M. A. Abdelkareem, and A. H. Al – Alami, “Critical review of energy storage systems,” *Energy*, vol. 214, Jan. 2021, doi: 10.1016/j.energy.2020.118987.
- [34] L. Wan *et al.*, “ZIF-8 derived nitrogen-doped porous carbon/carbon nanotube composite for high-performance supercapacitor,” *Carbon*, vol. 121, pp. 330–336, Sep. 2017, doi: 10.1016/j.carbon.2017.06.017.
- [35] M. D. Stoller, S. Park, Y. Zhu, J. An, and R. S. Ruoff, “Graphene-Based Ultracapacitors,” *Nano Letters*, vol. 8, no. 10, pp. 3498–3502, Oct. 2008, doi: 10.1021/nl802558y.
- [36] Vivekchand, S.R.C., Rout, C.S., Subrahmanyam, K.S. *et al.* “Graphene-based electrochemical supercapacitors”, *Journal of Chemical Sciences*, vol. 120, pp. 9–13, 2008, doi:10.1007/s12039-008-0002-7.
- [37] T. Kim, G. Jung, S. Yoo, K. S. Suh, and R. S. Ruoff, “Activated Graphene-Based Carbons as Supercapacitor Electrodes with Macro- and Mesopores,” *ACS Nano*, vol. 7, no. 8, pp. 6899–6905, Aug. 2013, doi: 10.1021/nn402077v.
- [38] A. Ghosh and Y. H. Lee, “Carbon-Based Electrochemical Capacitors,” *ChemSusChem*, vol. 5, no. 3, pp. 480–499, 2012, doi: 10.1002/cssc.201100645.
- [39] M. Cakici, R. R. Kakarla, and F. Alonso-Marroquin, “Advanced electrochemical energy storage supercapacitors based on the flexible carbon fiber fabric-coated with uniform coral-like MnO<sub>2</sub> structured electrodes,” *Chemical Engineering Journal*, vol. 309, pp. 151–158, Feb. 2017, doi: 10.1016/j.cej.2016.10.012.

- [40] Y.-K. Hsu, Y.-C. Chen, Y.-G. Lin, L.-C. Chen, and K.-H. Chen, “High-cell-voltage supercapacitor of carbon nanotube/carbon cloth operating in neutral aqueous solution,” *Journal of Material Chemistry*, vol. 22, no. 8, pp. 3383–3387, Jan. 2012, doi: 10.1039/C1JM14716A.
- [41] Q. Wang, W. Xia, W. Guo, L. An, D. Xia, and R. Zou, “Functional Zeolitic-Imidazolate-Framework-Templated Porous Carbon Materials for CO<sub>2</sub> Capture and Enhanced Capacitors,” *Chemistry – An Asian Journal*, vol. 8, no. 8, pp. 1879–1885, 2013, doi: 10.1002/asia.201300147.
- [42] R. R. Salunkhe *et al.*, “Fabrication of symmetric supercapacitors based on MOF-derived nanoporous carbons,” *Journal of Material Chemistry A*, vol. 2, no. 46, pp. 19848–19854, Nov. 2014, doi: 10.1039/C4TA04277H.
- [43] C. Young *et al.*, “Zeolitic imidazolate framework (ZIF-8) derived nanoporous carbon: the effect of carbonization temperature on the supercapacitor performance in an aqueous electrolyte,” *Physical Chemistry Chemical Physics*, vol. 18, no. 42, pp. 29308–29315, Oct. 2016, doi: 10.1039/C6CP05555A.
- [44] T. Gao, F. Zhou, W. Ma, and H. Li, “Metal-organic-framework derived carbon polyhedron and carbon nanotube hybrids as electrode for electrochemical supercapacitor and capacitive deionization,” *Electrochimica Acta*, vol. 263, pp. 85–93, Feb. 2018, doi: 10.1016/j.electacta.2018.01.044.
- [45] Y. Wang *et al.*, “ZIF-8@MWCNT-derived carbon composite as electrode of high performance for supercapacitor,” *Electrochimica Acta*, vol. 213, pp. 260–269, Sep. 2016, doi: 10.1016/j.electacta.2016.07.019.
- [46] Y. Zhang *et al.*, “All-solid-state asymmetric supercapacitors based on ZnO quantum dots/carbon/CNT and porous N-doped carbon/CNT electrodes derived from a single ZIF-8/CNT template,” *Journal of Material Chemistry A*, vol. 4, no. 26, pp. 10282–10293, Jun. 2016, doi: 10.1039/C6TA03633C.
- [47] Y. Liu, X. Xu, Z. Shao, and S. P. Jiang, “Metal-organic frameworks derived porous carbon, metal oxides and metal sulfides-based compounds for supercapacitors application,” *Energy Storage Materials*, vol. 26, pp. 1–22, Apr. 2020, doi: 10.1016/j.ensm.2019.12.019.

- [48] P. Zhang, F. Sun, Z. Shen, and D. Cao, "ZIF-derived porous carbon: a promising supercapacitor electrode material," *Journal of Material Chemistry A*, vol. 2, no. 32, pp. 12873–12880, Jul. 2014, doi: 10.1039/C4TA00475B.
- [49] L. Xin *et al.*, "Composites of hierarchical metal–organic framework derived nitrogen-doped porous carbon and interpenetrating 3D hollow carbon spheres from lotus pollen for high-performance supercapacitors," *New Journal of Chemistry*, vol. 41, no. 21, pp. 12835–12842, Oct. 2017, doi: 10.1039/C7NJ02427D.
- [50] R. R. Salunkhe *et al.*, "A high-performance supercapacitor cell based on ZIF-8-derived nanoporous carbon using an organic electrolyte," *Chemical Communications*, vol. 52, no. 26, pp. 4764–4767, Mar. 2016, doi: 10.1039/C6CC00413J.
- [51] S. Ratha and C. S. Rout, "Supercapacitor Electrodes Based on Layered Tungsten Disulfide-Reduced Graphene Oxide Hybrids Synthesized by a Facile Hydrothermal Method," *ACS Applied Materials and Interfaces*, vol. 5, no. 21, pp. 11427–11433, Nov. 2013, doi: 10.1021/am403663f.
- [52] E. G. da S. Firmiano *et al.*, "Supercapacitor Electrodes Obtained by Directly Bonding 2D MoS<sub>2</sub> on Reduced Graphene Oxide," *Advanced Energy Materials*, vol. 4, no. 6, 2014, doi: 10.1002/aenm.201301380.
- [53] K.-J. Huang, L. Wang, J.-Z. Zhang, L.-L. Wang, and Y.-P. Mo, "One-step preparation of layered molybdenum disulfide/multi-walled carbon nanotube composites for enhanced performance supercapacitor," *Energy*, vol. 67, pp. 234–240, Apr. 2014, doi: 10.1016/j.energy.2013.12.051.
- [54] K. Singh, S. Kumar, K. Agarwal, K. Soni, V. Ramana Gedela, and K. Ghosh, "Three-dimensional Graphene with MoS<sub>2</sub> Nanohybrid as Potential Energy Storage/Transfer Device," *Scientific Reports*, vol. 7, Aug. 2017, doi: 10.1038/s41598-017-09266-2.
- [55] B. Hu, X. Qin, A. M. Asiri, K. A. Alamry, A. O. Al-Youbi, and X. Sun, "Synthesis of porous tubular C/MoS<sub>2</sub> nanocomposites and their application as a novel electrode material for supercapacitors with excellent cycling stability," *Electrochimica Acta*, vol. 100, pp. 24–28, Jun. 2013, doi: 10.1016/j.electacta.2013.03.133.
- [56] X. Shang *et al.*, "Carbon fiber cloth supported interwoven WS<sub>2</sub> nanosheets with highly enhanced performances for supercapacitors," *Applied Surface Science*, vol. 392, pp. 708–714, Jan. 2017, doi: 10.1016/j.apsusc.2016.09.058.

- [57] K. Wang *et al.*, “General solution-processed formation of porous transition-metal oxides on exfoliated molybdenum disulfides for high-performance asymmetric supercapacitors,” *Journal of Material Chemistry A*, vol. 5, no. 22, pp. 11236–11245, Jun. 2017, doi: 10.1039/C7TA01457K.
- [58] L. Fang *et al.*, “Three-dimensional flower-like MoS<sub>2</sub>-CoSe<sub>2</sub> heterostructure for high performance supercapacitors,” *Journal of Colloid and Interface Science*, vol. 512, pp. 282–290, Feb. 2018, doi: 10.1016/j.jcis.2017.10.072.
- [59] L. Fang *et al.*, “Flower-like nanoarchitecture assembled from Bi<sub>2</sub>S<sub>3</sub> nanorod/MoS<sub>2</sub> nanosheet heterostructures for high-performance supercapacitor electrodes,” *Colloids and Surfaces A: Physicochemical and Engineering Aspects*, vol. 535, pp. 41–48, Dec. 2017, doi: 10.1016/j.colsurfa.2017.09.022.
- [60] H. Peng *et al.*, “High-Performance Asymmetric Supercapacitor Designed with a Novel NiSe@MoSe<sub>2</sub> Nanosheet Array and Nitrogen-Doped Carbon Nanosheet,” *ACS Sustainable Chemistry and Engineering*, vol. 5, no. 7, pp. 5951–5963, Jul. 2017, doi: 10.1021/acssuschemeng.7b00729.
- [61] L. Ren *et al.*, “Three-Dimensional Tubular MoS<sub>2</sub>/PANI Hybrid Electrode for High Rate Performance Supercapacitor,” *ACS Applied Material Interfaces*, vol. 7, no. 51, pp. 28294–28302, Dec. 2015, doi: 10.1021/acsami.5b08474.
- [62] Tang, H., Wang, J., Yin, H., Zhao, H., Wang, D. and Tang, Z., "Growth of Polypyrrole Ultrathin Films on MoS<sub>2</sub> Monolayers as High-Performance Supercapacitor Electrodes", *Advanced Materials*, vol. 27: pp. 1117-1123, doi: 10.1002/adma.201404622.
- [63] H. Zhang, M. A. Bork, K. J. Riedy, D. R. McMillin, and J. H. Choi, “Understanding Photophysical Interactions of Semiconducting Carbon Nanotubes with Porphyrin Chromophores,” *Journal of Physical Chemistry C*, vol. 118, no. 22, pp. 11612–11619, Jun. 2014, doi: 10.1021/jp503273d.
- [64] H. Zhang *et al.*, “DNA Oligonucleotide Templated Nanohybrids Using Electronic Type Sorted Carbon Nanotubes for Light Harvesting,” *Advanced Materials*, vol. 24, no. 40, pp. 5447–5451, 2012, doi: 10.1002/adma.201201628.

- [65] S. Manzetti and J.-C. P. Gabriel, “Methods for dispersing carbon nanotubes for nanotechnology applications: liquid nanocrystals, suspensions, polyelectrolytes, colloids and organization control,” *International Nano Letters*, vol. 9, no. 1, pp. 31–49, Mar. 2019, doi: 10.1007/s40089-018-0260-4.
- [66] H. Zhang *et al.*, “Regeneration of Light-Harvesting Complexes via Dynamic Replacement of Photodegraded Chromophores,” *ACS Applied Material Interfaces*, vol. 7, no. 15, pp. 7833–7837, Apr. 2015, doi: 10.1021/acsami.5b01924.
- [67] Q. Yue *et al.*, “A versatile ethanol-mediated polymerization of dopamine for efficient surface modification and the construction of functional core–shell nanostructures,” *Journal Material Chemistry B*, vol. 1, no. 44, pp. 6085–6093, Oct. 2013, doi: 10.1039/C3TB21028F.
- [68] B. A. Baker, H. Zhang, T.-G. Cha, and J. H. Choi, “9 - Carbon nanotube solar cells,” *Carbon Nanotubes and Graphene for Photonic Applications*, S. Yamashita, Y. Saito, and J. H. Choi, Eds. Woodhead Publishing, 2013, pp. 241–269.
- [69] K. Milburn, “Synthesis and Characterization of ZIF-8 and ZIF-8/polymer composites”, M.S. Thesis, Chem, Univ. of Liverpool, 2014, p. 154, [online].
- [70] Y. Gai, X. Chen, H. Yang, Y. Wang, X. Bu, and P. Feng, “A new strategy for constructing a disulfide-functionalized ZIF-8 analogue using structure-directing ligand–ligand covalent interaction,” *Chemical Communications*, vol. 54, no. 85, pp. 12109–12112, Oct. 2018, doi: 10.1039/C8CC07064D.
- [71] H. Zhang *et al.*, “Engineering Chemically Exfoliated Large-Area Two-Dimensional MoS<sub>2</sub> Nanolayers with Porphyrins for Improved Light Harvesting,” *ChemPhysChem*, vol. 17, no. 18, pp. 2854–2862, 2016, doi: 10.1002/cphc.201600511.
- [72] J. Choi *et al.*, “Nanomanufacturing of 2D Transition Metal Dichalcogenide Materials Using Self-Assembled DNA Nanotubes,” *Small*, vol. 11, no. 41, pp. 5520–5527, 2015, doi: 10.1002/smll.201501431.
- [73] X. J. Chua and M. Pumera, “The effect of varying solvents for MoS<sub>2</sub> treatment on its catalytic efficiencies for HER and ORR,” *Physical Chemistry Chemical Physics*, vol. 19, no. 9, pp. 6610–6619, Mar. 2017, doi: 10.1039/C6CP08205J.

- [74] J. Choi, H. Zhang, H. Du, and J. H. Choi, "Understanding Solvent Effects on the Properties of Two-Dimensional Transition Metal Dichalcogenides," *ACS Applied Material Interfaces*, vol. 8, no. 14, pp. 8864–8869, Apr. 2016, doi: 10.1021/acsami.6b01491.
- [75] J. Choi, H. Zhang, and J. H. Choi, "Modulating Optoelectronic Properties of Two-Dimensional Transition Metal Dichalcogenide Semiconductors by Photoinduced Charge Transfer," *ACS Nano*, vol. 10, no. 1, pp. 1671–1680, Jan. 2016, doi: 10.1021/acsnano.5b07457.
- [76] Q. Liu, T. L. Dzwiniel, K. Z. Pupek, and Z. Zhang, "Corrosion/Passivation Behavior of Concentrated Ionic Liquid Electrolytes and Its Impact on the Li-Ion Battery Performance," *Journal of the Electrochemical Society*, vol. 166, no. 16, Dec. 2019, doi: 10.1149/2.0161916jes.
- [77] S.-T. Myung, Y. Hitoshi, and Y.-K. Sun, "Electrochemical behavior and passivation of current collectors in lithium-ion batteries," *Journal of Material Chemistry*, vol. 21, no. 27, pp. 9891–9911, Jun. 2011, doi: 10.1039/C0JM04353B.
- [78] E. McCafferty, "Thermodynamics of Corrosion: Pourbaix Diagrams," *Introduction to Corrosion Science*, E. McCafferty, Ed. New York, NY: Springer, 2010, pp. 95–117.
- [79] L. Miao, Z. Song, D. Zhu, L. Li, L. Gan, and M. Liu, "Recent advances in carbon-based supercapacitors," *Materials Advances*, vol. 1, no. 5, pp. 945–966, 2020, doi: 10.1039/D0MA00384K.
- [80] N. C. Maile, S. K. Shinde, R. R. Koli, A. V. Fulari, D. Y. Kim, and V. J. Fulari, "Effect of different electrolytes and deposition time on the supercapacitor properties of nanoflake-like Co(OH)<sub>2</sub> electrodes," *Ultrasonics Sonochemistry*, vol. 51, pp. 49–57, Mar. 2019, doi: 10.1016/j.ultsonch.2018.09.003.
- [81] H. Ji *et al.*, "Capacitance of carbon-based electrical double-layer capacitors," *Nature Communications*, vol. 5, Art. no. 3317, Feb. 2014, doi: 10.1038/ncomms4317.
- [82] Xiao Li, Hongwei Zhu, "Two-dimensional MoS<sub>2</sub>: Properties, preparation, and applications", *Journal of Materiomics*, vol. 1, pp. 33-44, doi:10.1016/j.jmat.2015.03.003.
- [83] Patrick T Moseley, "High-rate, valve-regulated lead–acid batteries — suitable for hybrid electric vehicles?", *Journal of Power Sources*, Volume 84, Issue 2, 1999, Pages 237-242, doi:10.1016/S0378-7753(99)00323-7..

- [84] S. Pay and Y. Baghzouz, “Effectiveness of battery-supercapacitor combination in electric vehicles,” *2003 IEEE Bologna Power Tech Conference Proceedings*, Jun. 2003, vol. 3, p. 6, doi: 10.1109/PTC.2003.1304472.
- [85] A. Burke, Z. Liu, and H. Zhao, “Present and future applications of supercapacitors in electric and hybrid vehicles,” in *2014 IEEE International Electric Vehicle Conference (IEVC)*, Dec. 2014, pp. 1–8, doi: 10.1109/IEVC.2014.7056094.
- [86] T. Lé, P. Gentile, G. Bidan, and D. Aradilla, “New electrolyte mixture of propylene carbonate and butyltrimethylammonium bis(trifluoromethylsulfonyl)imide (N1114 TFSI) for high performance silicon nanowire (SiNW)-based supercapacitor applications,” *Electrochimica Acta*, vol. 254, pp. 368–374, Nov. 2017, doi: 10.1016/j.electacta.2017.09.147.
- [87] O. Tanaïke, D. N. Futaba, K. Hata, and H. Hatori, “Supercapacitors using Pure Single-walled Carbon Nanotubes,” *Carbon letters*, vol. 10, no. 2, pp. 90–93, Jun. 2009, doi: 10.5714/CL.2009.10.2.090.
- [88] A. Izadi-Najafabadi *et al.*, “High-Power Supercapacitor Electrodes from Single-Walled Carbon Nanohorn/Nanotube Composite,” *ACS Nano*, vol. 5, no. 2, pp. 811–819, Feb. 2011, doi: 10.1021/nn1017457.